
STOCHASTIC SIMULATION UNCERTAINTY ANALYSIS TO ACCELERATE FLEXIBLE BIOMANUFACTURING PROCESS DEVELOPMENT

Wei Xie^{*1}, Russell R. Barton², Barry L. Nelson³, and Keqi Wang¹

¹Department of Mechanical and Industrial Engineering, Northeastern University, MA, USA

²Supply Chain and Information Systems, Smeal College of Business, The Pennsylvania State University, PA, USA

³Department of Industrial Engineering and Management Sciences, IL, USA

ABSTRACT

Motivated by critical challenges and needs from biopharmaceuticals manufacturing, we propose a general metamodel-assisted stochastic simulation uncertainty analysis framework to accelerate the development of a simulation model with modular design for flexible production processes. There are often very limited process observations. Thus, there exist both simulation and model uncertainties in the system performance estimates. In biopharmaceutical manufacturing, model uncertainty often dominates. The proposed framework can produce a confidence interval that accounts for simulation and model uncertainties by using a metamodel-assisted bootstrapping approach. Furthermore, a variance decomposition is utilized to estimate the relative contributions from each source of model uncertainty, as well as simulation uncertainty. This information can be used to improve the system mean performance estimation. Asymptotic analysis provides theoretical support for our approach, while the empirical study demonstrates that it has good finite-sample performance.

Keywords Hybrid Simulation Model, Biomanufacturing Systems, Uncertainty Quantification (UQ), Sensitivity Analysis (SA), Gaussian Process (GP)

1 Introduction

While the biopharmaceutical industry has developed various innovative bio-drugs for severe diseases, such as cancers, autoimmune disorders, and infectious diseases, the current manufacturing systems are unable to rapidly produce new and existing drugs when needed, largely due to critical challenges, including high complexity, high variability, and very limited process data. Biotherapeutics are manufactured in living organisms (e.g., cells) whose biological processes are very complex. Manufacturing process typically consists of multiple integrated unit operations. There is often very limited data, i.e., having 3–20 process observations is typical in biomanufacturing [23], reflecting the high cost and long time needed to run lab experiments. Also, the more personalized nature of emerging bio-drugs (e.g., cell and gene therapies) makes it difficult to collect extensive data on every possible variety of drugs and every protein therapy can be unique, which often forces R&D efforts to work with just 3–5 batches.

Simulation can facilitate the development of flexible production systems with modular design. *Hybrid* (“*mechanistic+statistical*”) *simulation models* can support interpretable and robust decision making, while requiring much less data than purely data-based models. The mechanistic model parameters (such as cell growth rate, oxygen and nutrient uptake rates) can facilitate the learning of underlying biological/physical/chemical (a.k.a. *biophysicochemical*) mechanisms. Thus, in this paper, we suppose that the model family or structure, built on mechanism prior knowledge, is given. The model parameters are estimated from very limited real-world data, which introduces *model uncertainty*. When we create a simulation model to predict the performance of a real system, there exist the errors induced by both simulation estimation uncertainty and process model uncertainty.

In the biomanufacturing literature, modeling of bioprocess dynamics while considering different sources of uncertainty (e.g., batch-to-batch variations, measurement errors, and model uncertainty) is critical [25]. Model uncertainty

*Corresponding author: w.xie@northeastern.edu

quantification can be divided into frequentist and Bayesian approaches. In frequentist inference, model parameter estimation uncertainty is typically quantified via a confidence interval or standard deviation [22, 34]. In Bayesian inference, posterior distributions are used to quantify and update model uncertainty [13, 38].

This study is directly related to the existing frequentist and Bayesian approaches on uncertainty quantification and sensitivity analysis; see recent reviews in [9, 8]. The Bayesian approaches typically use the posterior distributions of inputs given the real-world data to quantify the input distribution uncertainty; see for example [41, 42, 6]. Direct bootstrapping, as frequentist approach, quantifies the impact of input uncertainty using bootstrap resampling of the input data and runs simulations at each bootstrap resample point to estimate the impact on the system mean [5, 4]. Compared with the Bayesian approaches, the direct bootstrap can be adapted to any input process without additional analysis (e.g., posterior distribution derivation). The metamodel-assisted bootstrapping approach is further introduced by [3]. In this framework, the uncertainty is propagated to the output mean by a metamodel, which can be constructed using simulation results from a small number of runs. Thus, this method does not need substantial computational effort.

Built on [3], we propose a metamodel-assisted uncertainty quantification and sensitivity analysis (UQ&SA) framework to accelerate the development of flexible manufacturing process with modular design. As a result we can form a confidence interval (CI) quantifying the overall estimation uncertainty of the system’s mean performance. Specifically, bootstrap resampling of the real-world data is used to approximate the model uncertainty. Then, a Gaussian process (GP) metamodel is used to propagate the heterogeneous process model uncertainty to the output mean response. Since model uncertainty typically dominates in the biopharmaceutical manufacturing processes, we further develop sensitivity analysis to quantify the contribution from each source of model uncertainty.

The key contributions of this study are threefold.

- First, we introduce a metamodel-assisted uncertainty quantification (UQ) and sensitivity analysis (SA) framework for hybrid model based simulations. The proposed algorithm can deliver a percentile CI of system mean response, accounting for both model and simulation uncertainties. A further sensitivity analysis can provide the relative contribution from each source of uncertainty. Differing with existing simulation studies in the literature that typically consider the simulation model as a black-box (see for example the review paper [9]), hybrid model based simulation can leverage existing mechanistic models, facilitate mechanism learning, and support interpretable decision making.
- Second, under the assumption that the unknown mean response surface is a realization of GP, which is a useful representation in many problems, we provide a systematic asymptotic analysis on the proposed GP metamodel assisted UQ and SA framework, including (1) the asymptotic consistency of the proposed CI; and (2) the asymptotic consistency of variance estimators quantifying each source of model uncertainty and simulation uncertainty.
- Third, we provide a comprehensive empirical study to show that the proposed framework has promising finite sample performance, especially under situations with very limited real-world data.

Some existing simulation methodologies can be integrated into the proposed framework to support extensions for computational saving and system risk performance assessment, such as measured by quantiles. Considering the total simulation cost required to achieve consistent estimation of model uncertainty when using the conventional bootstrap resampling techniques, [16, 17] proposed the subsampling techniques as a computational saver to promote the computational efficiency. In addition, the proposed UQ and SA framework can be extended to system quantile performance measure through GP based percentile regression; see for example [40, 39, 37].

The remainder of the paper is organized as follows. We present the problem description in Section 2 and give a brief review of the metamodel-assisted bootstrapping approach in Section 3. In Section 4, we provide an algorithm to build an interval quantifying the overall estimation uncertainty of system mean performance, accounting for both model and simulation uncertainties. Then, we provide a variance decomposition approach to estimate the relative contribution from each source of model uncertainty, as well as simulation uncertainty. We provide an empirical study in Section 5 and conclude the paper in Section 6. All proofs are provided in the Appendix.

2 Problem Description and Proposed Framework

A typical biomanufacturing system consists of multiple unit operations, including upstream fermentation for drug substance production and downstream purification to meet quality requirements [11]. It can consist of numerous unit operations; see an example illustrated in Figure 1. Operations typically include (1) fermentation, (2) centrifugation, (3) chromatography, (4) filtration, and (5) quality control. Operation unit (1) belongs to upstream cell culture and target drug substance production process, and (2)–(5) belong to downstream purification process.

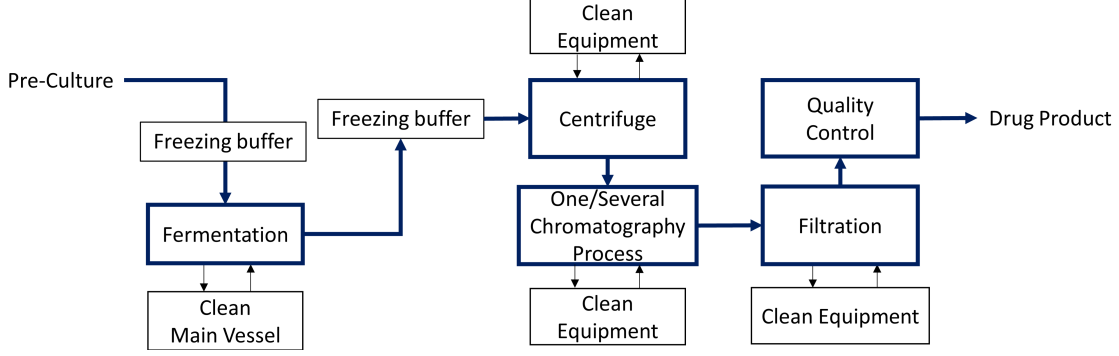


Figure 1: An illustrative example of integrated biomanufacturing process.

To guide reliable and interpretable decision making, a simulation model can be developed based on hybrid models of modules defined according to bioprocess biophysicochemical mechanisms, dynamics, and interdependence of mechanistic parameters. Given very limited real-world data, we take existing mechanistic models as prior knowledge on the structure of mechanism relationships and create *parametric hybrid models*. It can leverage the advantages of mechanistic and statistical models to facilitate mechanism learning and improve sample efficiency and decision interpretability.

The fermentation is the most critical operation unit in the production process and it determines the generation of target drug substance (such as protein monoclonal antibodies or mAbs) and impurities. Here we use a simple example of fermentation on protein production to illustrate bioprocess hybrid modeling. Specifically, the target protein and biomass generation in the exponential-growth phase of fermentation process can be modeled with the cell-growth kinetics mechanism [11]. Built on it, we construct a hybrid model capturing bioprocess dynamics and variation, i.e.,

$$X_t = X_0 \cdot e^{\gamma t} + \epsilon_P, \quad (1)$$

where X_t represents the biomass concentration at time t and the growth rate, denoted by γ , depends on biological properties of working cells and culture environments. We model batch-to-batch variation on: (1) the specific growth rate as $\gamma \sim N(\mu_\gamma, \sigma_\gamma^2)$; and (2) raw materials or initial concentration of seed cells as $X_0 \sim N(\mu_0, \sigma_0^2)$. In addition, we model the measurement error or residual as $\epsilon_P \sim N(0, \sigma_P^2)$ to capture the integrated impact from ignored factors. Larger variance from the residual indicates less understanding on underlying bioprocessing mechanisms obtained from the existing exponential growth mechanistic model. Thus, the distributions of residual ϵ_P , protein growth rate γ_P , and raw materials X_0 uniquely characterize the hybrid model of target protein accumulation during the fermentation process.

The normality assumption is often used in the biopharmaceutical literature to model batch-to-batch variations and measurement errors since they are often induced by many underlying factors; see for example [21]. In addition, there is often very limited data. In our previous study, we used real-world fermentation process data with the size of 8 batches to conduct the hypothesis test which validates the normality assumption [38].

An integrated biomanufacturing system is often composed of multiple interconnected modules. Suppose that the simulation model is a function of L parametric multivariate and univariate models $F \equiv \{F_1, F_2, \dots, F_L\}$ characterizing the underlying bioprocess dynamics and variations. Each ℓ -th model F_ℓ can be uniquely characterized by h_ℓ unknown parameters. In the simple fermentation example mentioned above in (1), the variation of residual ϵ_P is characterized by model F_1 specified by parameter σ_P^2 ; the batch-to-batch variation on the growth rate γ is characterized by model F_2 specified by parameters $\{\mu_\gamma, \sigma_\gamma^2\}$ and the raw material uncertainty is characterized by model F_3 specified by parameters $\{\mu_0, \sigma_0^2\}$.

Each h_ℓ -parameter distribution is uniquely specified by its first (finite) h_ℓ moments, which is true for the distributions that are most often used in stochastic simulation. The moments are chosen as the input variables for the metamodel of the system response surface because when they are close, the corresponding distributions will be similar and therefore generate similar outputs. Let $\mathbf{x}_{[\ell]}$ denote an $h_\ell \times 1$ vector of the first h_ℓ moments for the ℓ -th model and $d = \sum_{\ell=1}^L h_\ell$. Then, by stacking $\mathbf{x}_{[\ell]}$ with $\ell = 1, 2, \dots, L$ together, we have a $d \times 1$ dimensional input vector, denoted by \mathbf{x} . Notice that $F = \{F_1, F_2, \dots, F_L\}$ is completely characterized by the collection of model moments $\mathbf{x} = (\mathbf{x}_{[1]}, \mathbf{x}_{[2]}, \dots, \mathbf{x}_{[L]})^\top$.

The output from the j -th replication of a simulation with model moments \mathbf{x} can be written as

$$Y_j(\mathbf{x}) = \mu(\mathbf{x}) + \epsilon_j(\mathbf{x}) \quad (2)$$

where $\mu(\mathbf{x}) = E[Y_j(\mathbf{x})]$ denotes the unknown expected performance (e.g., productivity of protein drug substance) and $\epsilon_j(\mathbf{x})$ represents the simulation error with mean zero. The simulation output depends on the choice of process models. Let $\Psi \equiv \{\mathbf{x} \in \mathbb{R}^d: \text{the random variable } Y(\mathbf{x}) \text{ is defined and } \mu(\mathbf{x}) \text{ is finite}\}$ denote the region of interest. We assume $\mu(\mathbf{x})$ is continuous for $\mathbf{x} \in \Psi$.

The underlying ‘‘correct’’ process models, denoted by $F^c \equiv \{F_1^c, F_2^c, \dots, F_L^c\}$, specified by the moments, $\mathbf{x}_c = (\mathbf{x}_{[1],c}, \mathbf{x}_{[2],c}, \dots, \mathbf{x}_{[L],c})$, are unknown and are estimated from a finite sample of real-world data. Suppose that the set of true parameters \mathbf{x}_c is in the interior of Ψ . Our goal is to find a $(1 - \alpha)100\%$ CI, denoted by $[Q_L, Q_U]$, such that

$$\Pr\{\mu(\mathbf{x}_c) \in [Q_L, Q_U]\} = 1 - \alpha, \quad (3)$$

which quantifies the overall estimation uncertainty of system mean performance, accounting for simulation and model uncertainties. Then, if this interval is too wide, we further develop a variance decomposition to quantify the contribution from each source of model uncertainty, which can guide more data collection and improve the system mean response estimation.

The true moments \mathbf{x}_c are unknown and estimated based on a finite sample \mathbf{Z}_m from F^c . Let m_ℓ denote the number of i.i.d. real-world observations available from the ℓ -th model, i.e., $\mathbf{Z}_{\ell, m_\ell} \equiv \{Z_{\ell,1}, Z_{\ell,2}, \dots, Z_{\ell, m_\ell}\}$ with $Z_{\ell, i} \stackrel{i.i.d.}{\sim} F_\ell^c$, $i = 1, 2, \dots, m_\ell$. Let $\mathbf{Z}_m = \{\mathbf{Z}_{\ell, m_\ell}, \ell = 1, 2, \dots, L\}$ be the collection of samples from all L model distributions in F^c , where $\mathbf{m} = (m_1, m_2, \dots, m_L)$. Let \mathbf{X}_m be a $d \times 1$ dimensional moment estimator that is a function of \mathbf{Z}_m written as $\mathbf{X}_m = \mathbf{X}(\mathbf{Z}_m)$. Specifically, $\mathbf{X}_{\ell, m_\ell} = \mathbf{X}_\ell(\mathbf{Z}_{\ell, m_\ell})$ and $\mathbf{X}_m^T = (\mathbf{X}_{1, m_1}^T, \mathbf{X}_{2, m_2}^T, \dots, \mathbf{X}_{L, m_L}^T)$. Let $F_{\mathbf{X}_m}^c$ represent the true, unknown distribution of \mathbf{X}_m . Therefore, the impact of model uncertainty is captured by the sampling distribution of $\mu(\mathbf{X}_m)$ with $\mathbf{X}_m \sim F_{\mathbf{X}_m}^c$. The real-world data are a particular realization of \mathbf{Z}_m , say $\mathbf{z}_m^{(0)}$. Given a finite sample of real-world data $\mathbf{z}_m^{(0)}$, we use bootstrap resampling to approximate $F_{\mathbf{X}_m}^c$ and a metamodel to represent $\mu(\mathbf{x})$. Notice that the components of the moment estimator \mathbf{X}_m can be statistically dependent.

Suppose each experiment is expensive. The proposed metamodel-assisted bootstrapping uncertainty analysis framework can accelerate the development of a simulation model for a flexible and integrated real manufacturing system with modular design. Since the underlying response surface $\mu(\cdot)$ is unknown, we model our prior belief about $\mu(\cdot)$ by a Gaussian Process (GP). Given a set of stochastic simulation outputs, the GP-based belief is updated by a posterior distribution, denoted by $M_p(\cdot)$. When we use this metamodel to propagate the sampling distribution of \mathbf{X}_m to the output mean, it introduces the simulation uncertainty induced by finite simulation runs (i.e., finite design points and finite run length in each simulation run). *Thus, the estimation uncertainty of underlying system mean performance $\mu(\mathbf{x}_c)$ is characterized by the compound random variable, $M_p(\mathbf{X}_m)$, accounting for both model and simulation uncertainties.* Based on the variability of $M_p(\mathbf{X}_m)$, we can construct an interval estimator $[Q_L, Q_U]$ in (3) to quantify the overall estimation uncertainty of real system mean response $\mu(\mathbf{x}_c)$.

We further develop a variance decomposition measuring the contributions to $\text{Var}[M_p(\mathbf{X}_m)]$ from simulation uncertainty quantified by GP $M_p(\cdot)$ and model uncertainty quantified by the sampling distribution of $\mathbf{X}_m^T = (\mathbf{X}_{1, m_1}^T, \mathbf{X}_{2, m_2}^T, \dots, \mathbf{X}_{L, m_L}^T)$. Therefore, if this interval is too wide, our study can guide further data collection to efficiently update the simulation model to faithfully represent the real system and improve the estimation accuracy of $\mu(\mathbf{x}_c)$.

If the simulation uncertainty dominates, we will allocate more computational resource to improve our knowledge on the mean response surface $\mu(\cdot)$. However, in biopharmaceutical manufacturing with high stochasticity and very limited process observations, model uncertainty often dominates. The distribution of model uncertainty depends on heterogeneous process observations, as well as the complexity of the underlying mechanisms and inherent stochasticity at each part of the integrated biomanufacturing system. Thus, if certain model uncertainty, say $\mathbf{X}_{\ell, m_\ell}$ with $\ell = 1, 2, \dots, L$, dominates the system performance estimation uncertainty, it will guide us collecting the additional real-world data there to improve the simulation model.

3 Metamodel-Assisted Bootstrapping for Uncertainty Quantification

We introduce the metamodel-assisted bootstrapping and provide the algorithm for uncertainty analysis. Basically, we first find the space-filling design points covering the most likely bootstrap samples of model moments, denoted by $\widehat{\mathbf{X}}_m^{(b)}$ with $b = 1, 2, \dots, B$, quantifying the model uncertainty. Then, we run simulations and construct the GP or stochastic kriging (SK) metamodel for the mean response surface $\mu(\cdot)$ quantifying simulation uncertainty in Section 3.1. This

metamodel is used to propagate the model uncertainty to output mean. We introduce the metamodel-assisted bootstrapping in Section 3.2 to construct an interval of $\mu(\mathbf{x}_c)$ accounting for both simulation and model uncertainties, and show its asymptotic consistency in Section 3.3.

3.1 Stochastic Kriging Metamodel

Since the outputs from simulations include simulation variability that often changes significantly across the design space of process models specified by moments \mathbf{x} , SK is introduced to distinguish the uncertainty about the response surface from the simulation uncertainty [2, 15]. Suppose that the underlying unknown response surface can be thought of as a realization of a stationary GP. The simulation output Y is modeled as,

$$Y_j(\mathbf{x}) = \beta_0 + W(\mathbf{x}) + \epsilon_j(\mathbf{x}) \quad (4)$$

where \mathbf{x} denotes a $d \times 1$ vector of model moments. SK uses a mean-zero, second-order stationary GP $W(\mathbf{x})$ to account for the spatial dependence of the response surface. Thus, the uncertainty about the true response surface $\mu(\mathbf{x})$ is represented by a GP $M(\mathbf{x}) \equiv \beta_0 + W(\mathbf{x})$ (note that β_0 can be replaced by a more general trend term $\mathbf{f}(\mathbf{x})^\top \boldsymbol{\beta}$). For many, but not all, simulation settings the output is an average of a large number of more basic outputs, so a normal approximation can be applied: $\epsilon(\mathbf{x}) \sim \mathcal{N}(0, \sigma_\epsilon^2(\mathbf{x}))$.

In SK, the covariance between $W(\mathbf{x})$ and $W(\mathbf{x}')$ quantifies how knowledge of the surface at some design points affects the prediction of the surface. A parametric form of the spatial covariance, denoted by $\Sigma(\mathbf{x}, \mathbf{x}') = \text{Cov}[W(\mathbf{x}), W(\mathbf{x}')] = \tau^2 r(\mathbf{x} - \mathbf{x}')$, is typically assumed where τ^2 denotes the variance and $r(\cdot)$ is a correlation function that depends only on the distance $\mathbf{x} - \mathbf{x}'$. Based on our previous study [36], we use the product-form Gaussian correlation function $r(\mathbf{x} - \mathbf{x}') = \exp(-\sum_{j=1}^d \theta_j (x_j - x'_j)^2)$ for the empirical evaluation in Section 5. Let $\boldsymbol{\theta} = (\theta_1, \theta_2, \dots, \theta_d)$ represent the correlation parameters. Thus, the prior knowledge of the response surface $\mu(\mathbf{x})$ is represented by a Gaussian process, i.e., $M(\mathbf{x}) \sim \text{GP}(\beta_0, \tau^2 r(\mathbf{x} - \mathbf{x}'))$.

To reduce the uncertainty about $\mu(\mathbf{x})$, we choose an experiment design consisting of pairs $\mathcal{D} \equiv \{(\mathbf{x}_i, n_i), i = 1, 2, \dots, k\}$ at which to run simulations and collect observations, where (\mathbf{x}_i, n_i) denotes the location and the number of replications, respectively, at the i -th design point. The design that we recommend is described in more detail in D. The simulation outputs at \mathcal{D} are $\mathbf{Y}_{\mathcal{D}} \equiv \{(Y_1(\mathbf{x}_i), Y_2(\mathbf{x}_i), \dots, Y_{n_i}(\mathbf{x}_i)); i = 1, 2, \dots, k\}$ and the sample mean at design point \mathbf{x}_i is $\bar{Y}(\mathbf{x}_i) = \sum_{j=1}^{n_i} Y_j(\mathbf{x}_i)/n_i$. Let the sample means at all k design points be $\bar{\mathbf{Y}}_{\mathcal{D}} = (\bar{Y}(\mathbf{x}_1), \bar{Y}(\mathbf{x}_2), \dots, \bar{Y}(\mathbf{x}_k))^T$. Set the simulations at different design points independent. Then, the variance of $\bar{\mathbf{Y}}_{\mathcal{D}}$ is represented by a $k \times k$ diagonal matrix $C = \text{diag}\{\sigma_\epsilon^2(\mathbf{x}_1)/n_1, \sigma_\epsilon^2(\mathbf{x}_2)/n_2, \dots, \sigma_\epsilon^2(\mathbf{x}_k)/n_k\}$.

Let Σ be the $k \times k$ spatial covariance matrix of the design points and let $\Sigma(\mathbf{x}, \cdot)$ be the $k \times 1$ spatial covariance vector between the design points and a fixed prediction point \mathbf{x} . If the parameters $(\tau^2, \boldsymbol{\theta}, C)$ are known, then the metamodel or simulation uncertainty can be characterized by a refined GP $M_p(\mathbf{x})$ that denotes the conditional distribution of $M(\mathbf{x})$ given simulation outputs $\bar{\mathbf{Y}}_{\mathcal{D}}$,

$$M_p(\mathbf{x}) \sim \text{GP}(m_p(\mathbf{x}), \sigma_p^2(\mathbf{x})) \quad (5)$$

where the minimum mean squared error (MSE) linear unbiased predictor is

$$m_p(\mathbf{x}) = \hat{\beta}_0 + \Sigma(\mathbf{x}, \cdot)^\top (\Sigma + C)^{-1} (\bar{\mathbf{Y}}_{\mathcal{D}} - \hat{\beta}_0 \cdot \mathbf{1}_{k \times 1}), \quad (6)$$

and the corresponding variance is

$$\begin{aligned} \sigma_p^2(\mathbf{x}) &= \tau^2 - \Sigma(\mathbf{x}, \cdot)^\top (\Sigma + C)^{-1} \Sigma(\mathbf{x}, \cdot) \\ &\quad + \eta^\top [\mathbf{1}_{k \times 1}^\top (\Sigma + C)^{-1} \mathbf{1}_{k \times 1}]^{-1} \eta \end{aligned} \quad (7)$$

where $\hat{\beta}_0 = [\mathbf{1}_{k \times 1}^\top (\Sigma + C)^{-1} \mathbf{1}_{k \times 1}]^{-1} \mathbf{1}_{k \times 1}^\top (\Sigma + C)^{-1} \bar{\mathbf{Y}}_{\mathcal{D}}$ and $\eta = 1 - \mathbf{1}_{k \times 1}^\top (\Sigma + C)^{-1} \Sigma(\mathbf{x}, \cdot)$ [2]. The spatial correlation parameters τ^2 and $\boldsymbol{\theta}$ are estimated by using MLEs. The sample variance is used as an estimate for the simulation variance at design points C . By plugging $(\hat{\beta}_0, \hat{\tau}^2, \hat{\boldsymbol{\theta}}, \hat{C})$ into Equations (6) and (7), we can obtain the estimated mean $\hat{m}_p(\mathbf{x})$ and variance $\hat{\sigma}_p^2(\mathbf{x})$. Thus, the metamodel we use is $\hat{\mu}(\mathbf{x}) = \hat{m}_p(\mathbf{x})$ with marginal variance estimated by $\hat{\sigma}_p^2(\mathbf{x})$.

[2] demonstrate that $\hat{m}_p(\mathbf{x})$ is still an unbiased predictor even with the plug-in estimator \hat{C} , and the variance inflation of $\hat{\sigma}_p^2(\mathbf{x})$ caused by using \hat{C} is typically small. In the asymptotic analysis, we assume that the parameters $(\tau^2, \boldsymbol{\theta}, C)$ are known. This is necessary (and common in the kriging literature) because including the effect of parameter estimation is mathematically intractable. Further, there is both theoretical and empirical evidence that in many cases prediction accuracy is minimally affected by using estimated hyperparameters; see [35].

3.2 Metamodel-Assisted Bootstrapping for Uncertainty Quantification

The proposed metamodel-assisted bootstrapping can provide a CI for the true mean performance, which accounts for both model and simulation uncertainties. Since $m_p(\mathbf{x})$ is an unbiased predictor under the GP assumption, $\sigma_p^2(\mathbf{x}) = 0$ for all \mathbf{x} would imply that there is no simulation uncertainty due either to a finite number of design points \mathbf{x}_i or finite number of replications n_i ; that is, $m_p(\mathbf{x}) = \mu(\mathbf{x})$. Unfortunately, if the budget is tight relative to the complexity of the true response surface, then the effect of simulation uncertainty could be substantial, resulting in significant undercoverage of the confidence interval of [3] as we show in Section 5. The new interval introduced here does not suffer this degradation, and therefore is robust to the amount of simulation effort that can be expended.

The kriging literature is the foundation for our work; see for instance [26]. Kriging models uncertainty about the function as a GP $M(\cdot)$ by assuming $\mu(\cdot)$ is a realization of $M(\cdot)$. An interval constructed to cover the conditional distribution of $M(\mathbf{x}_0)$ given the values at the design points is often interpreted as a CI for $\mu(\mathbf{x}_0)$; see for example [24]. The success of this paradigm is not because the function of interest is actually random—it is not—but because in many problems the conditional GP appears to be a robust characterization of the remaining response-surface uncertainty.

We adopt the kriging paradigm but with two key differences: our prediction point \mathbf{x}_c is unknown and must be estimated from real-world data, and our function $\mu(\cdot)$ can only be evaluated in the presence of stochastic simulation noise. Given the simulation outputs $\bar{\mathbf{Y}}_{\mathcal{D}}$, the remaining uncertainty about $\mu(\cdot)$ is characterized by the conditional GP $M_p(\cdot)$. To account for the impact from both model and simulation uncertainties, we construct an interval $[C_L, C_U]$ covering $M_p(\mathbf{x}_c)$ with probability $(1 - \alpha)100\%$, i.e.,

$$\Pr\{M_p(\mathbf{x}_c) \in [C_L, C_U]\} = 1 - \alpha. \quad (8)$$

Since the conditional coverage is $1 - \alpha$, the unconditional coverage of $M(\mathbf{x}_c)$ is $1 - \alpha$ as well. *The revised objective (8) is connected to our objective (3) through the assumption that the function $\mu(\cdot)$ is a realization of the GP $M(\cdot)$.* A procedure that delivers an interval satisfying (8) will be a good approximation for a CI procedure satisfying (3) if $M_p(\cdot)$ faithfully represents the remaining uncertainty about $\mu(\cdot)$. This is clearly an approximation because in any real problem $\mu(\cdot)$ is a fixed function, therefore we refer to $[C_L, C_U]$ as an approximation for the CI (ACI).

Based on a hierarchical approach, we propose Algorithm 1 to build $(1 - \alpha)100\%$ bootstrap percentile ACIs to achieve (8). In this procedure, Step 1 provides an experiment design to build a SK metamodel, which is central to the metamodel-assisted bootstrapping approach. Since the system model uncertainty is quantified with bootstrapped samples, we want the metamodel to correctly predict the responses at these sample points $\hat{\mathbf{X}}_{\mathbf{m}} \sim \hat{F}_{\mathbf{X}_{\mathbf{m}}}(\cdot | \mathbf{z}_{\mathbf{m}}^{(0)})$. Thus, the metamodel needs to be accurate and precise in a design space that covers the “most likely” bootstrap moment estimates, which can be achieved by the experiment design proposed by [3]. Specifically, they find the smallest ellipsoid denoted by E that covers the most likely bootstrap resampled moments and then generate a space-filling design that covers E ; see the details in Appendix D.

Based on the experiment design provided in Step 1, we run simulations and construct a metamodel in Step 2 by fitting $(\beta_0, \tau^2, \boldsymbol{\theta}, C)$. Given the metamodel, we predict the simulation’s mean responses at different model settings corresponding to bootstrap resampled moments. The bootstrap resampled moments are drawn from the bootstrap distribution denoted by $\hat{F}_{\mathbf{X}_{\mathbf{m}}}(\cdot | \mathbf{z}_{\mathbf{m}}^{(0)})$. In Step 3(a), we generate bootstrapped model moments. Then, we return a $(1 - \alpha)100\%$ interval estimators as shown in Algorithm 1. Notice that Step 3(b) accounts for the model uncertainty and Step 3(c) accounts for the simulation uncertainty. Thus, this procedure provides two types of intervals: **(a)** CI_0 , proposed in [3], returns an estimate of $[Q_L, Q_U]$ in eq. (3) by assuming $\hat{m}_p(\mathbf{x}) = \mu(\mathbf{x})$; that is, it only accounts for model uncertainty and will be in error if there is substantial simulation uncertainty. **(b)** CI_+ returns an estimate of $[C_L, C_U]$ in eq. (8). This ACI accounts for both model and simulation uncertainty. As the simulation uncertainty decreases, CI_0 and CI_+ become closer and closer to each other. Before evaluating the finite-sample performance of CI_+ in Section 5, we establish its asymptotic consistency for objective (8) in Section 3.3. Then, in Steps 4 and 5, variance decomposition is developed to quantify the contribution from each source of uncertainty, which will be studied in Section 4.

3.3 Asymptotic Consistency Study on Interval CI_+

In this section, we show that the ACI CI_+ provided in Algorithm 1 satisfies Equation (8) asymptotically. *The asymptotic consistency of this interval is proved under the assumption that the true response surface $\mu(\mathbf{x})$ is a realization of a GP with all parameters known except β_0 .* Under this assumption, $M_p(\mathbf{x})$ characterizes the remaining simulation uncertainty after observing $\bar{\mathbf{Y}}_{\mathcal{D}}$. Since the model uncertainty is asymptotically correctly quantified by the bootstrap moment estimator $\hat{\mathbf{X}}_{\mathbf{m}}$, the distribution of $M_p(\hat{\mathbf{X}}_{\mathbf{m}})$ accounts for both model and simulation uncertainties. Theorem 3.1 shows that this interval satisfies objective (8) asymptotically. The detailed proof is provided in Appendix B.

Algorithm 1: Metamodel-Assisted Bootstrap for Uncertainty Quantification and Sensitivity Analysis

Input: Given real-world data $\mathbf{z}_m^{(0)} = \{\mathbf{z}_{\ell, m_\ell}^{(0)}, \ell = 1, 2, \dots, L\}$

Output: Estimated CI and ACI quantifying the overall estimation uncertainty of $\mu(\mathbf{x}_c)$; Estimated model variance $\hat{\sigma}_I^2$, simulation variance $\hat{\sigma}_M^2$ and uncertainty contribution \hat{s}_ℓ from ℓ -th model.

Function of Uncertainty Quantification (UQ):

Step 1: Build the design space covering the most likely bootstrap moment estimates of process models, and choose a space-filling experiment design $\mathcal{D} = \{(\mathbf{x}_i, n_i), i = 1, 2, \dots, k\}$ as described in Appendix D.

Step 2: Run simulations at design points to obtain outputs $\mathbf{Y}_\mathcal{D}$. Compute the sample average $\bar{Y}(\mathbf{x}_i)$ and sample variance $S^2(\mathbf{x}_i)$ of the simulation outputs, $i = 1, 2, \dots, k$. Fit the SK metamodel parameters $(\beta_0, \tau^2, \boldsymbol{\theta}, C)$ to obtain $\hat{m}_p(\mathbf{x})$ and $\hat{\sigma}_p^2(\mathbf{x})$ using $(\bar{Y}(\mathbf{x}_i), S^2(\mathbf{x}_i), \mathbf{x}_i), i = 1, 2, \dots, k$.

Step 3: for $b = 1$ to B do

Step 3(a): Draw m_ℓ samples with replacement from $\mathbf{z}_{\ell, m_\ell}^{(0)}$, denoted by $\mathbf{Z}_{\ell, m_\ell}^{(b)}$, and calculate the corresponding $h_\ell \times 1$ vector of bootstrap moment estimates denoted by $\hat{\mathbf{X}}_{\ell, m_\ell}^{(b)} = \mathbf{X}_\ell(\mathbf{Z}_{\ell, m_\ell}^{(b)})$ for $\ell = 1, 2, \dots, L$. Then stack the results for all L processes to obtain a $d \times 1$ vector $\hat{\mathbf{X}}_m^{(b)}$.

Step 3(b): Let $\hat{\mu}_b \equiv \hat{m}_p(\hat{\mathbf{X}}_m^{(b)})$.

Step 3(c): Draw $\hat{M}_b \sim N(\hat{m}_p(\hat{\mathbf{X}}_m^{(b)}), \hat{\sigma}_p^2(\hat{\mathbf{X}}_m^{(b)}))$.

Return (1) Estimated $(1 - \alpha)100\%$ bootstrap percentile CI and ACI; **(2)** Estimated model variance and simulation variance,

$$\text{CI}_0 = \left[\hat{\mu}_{(\lceil B \frac{\alpha}{2} \rceil)}, \hat{\mu}_{(\lceil B(1 - \frac{\alpha}{2}) \rceil)} \right], \quad \text{CI}_+ = \left[\hat{M}_{(\lceil B \frac{\alpha}{2} \rceil)}, \hat{M}_{(\lceil B(1 - \frac{\alpha}{2}) \rceil)} \right],$$

$$\hat{\sigma}_I^2 = \sum_{b=1}^B (\hat{\mu}_b - \hat{\mu})^2 / (B - 1), \quad \hat{\sigma}_M^2 = \sum_{b=1}^B \hat{\sigma}_p^2(\hat{\mathbf{X}}_m^{(b)}) / B,$$

where $\hat{\mu}_{(1)} \leq \hat{\mu}_{(2)} \leq \dots \leq \hat{\mu}_{(B)}$ and $\hat{M}_{(1)} \leq \hat{M}_{(2)} \leq \dots \leq \hat{M}_{(B)}$ are the sorted values, and $\hat{\mu} = \sum_{b=1}^B \hat{\mu}_b / B$.

Function of Sensitivity Analysis (SA):

for each $\mathcal{J} \subseteq \mathcal{L}$ with $\mathcal{L} = \{1, 2, \dots, L\}$ do

Step 4: Generate bootstrap samples $\hat{\mathbf{X}}_\mathcal{J}^{(b)}$ for $b = 1, 2, \dots, B'$ and obtain simulation output prediction $\hat{m}_p(\mathbf{x}_{-\mathcal{J}}^{(0)}, \hat{\mathbf{X}}_\mathcal{J}^{(b)})$.

Step 5: Estimate the cost function $c(\mathcal{J})$ by (13).

Return Estimated ℓ th model uncertainty contribution \hat{s}_ℓ through (12) with $\ell = 1, 2, \dots, L$.

Theorem 3.1. Suppose that Assumptions (\star) in Appendix A hold. Then the interval $\text{CI}_+ = [M_{(\lceil B \frac{\alpha}{2} \rceil)}, M_{(\lceil B(1 - \frac{\alpha}{2}) \rceil)}]$ is asymptotically consistent,

$$\lim_{m \rightarrow \infty} \lim_{B \rightarrow \infty} \Pr\{M_{(\lceil B \alpha / 2 \rceil)} \leq M_p(\mathbf{x}_c) \leq M_{(\lceil B(1 - \alpha / 2) \rceil)}\} = 1 - \alpha. \quad (9)$$

4 Variance Decomposition for Uncertainty Analysis

In a practical setting, what is the next step if the interval CI_+ is so wide that we are uncomfortable making decisions based on estimates with that level of error? We suggest gaining some sense of the relative contribution from each source of uncertainty as a guide toward either collecting more real-world process data to reduce the model uncertainty or running more simulations to improve the system mean response estimation at any given models F . The overall estimation variance of system true performance $\mu(\mathbf{x}_c)$ is quantified by $\text{Var}[M_p(\mathbf{X}_m)]$. In Section 4.1, we propose a variance decomposition approach to quantify the contribution from simulation and model uncertainties. Compared with the existing studies on estimating the relative contributions, such as [30], our variance decomposition does not require the homogeneity assumption, i.e., the simulation noise has a constant variance. Since the effect of model uncertainty is induced by the complex interactions of estimation uncertainties from L models (F_1, F_2, \dots, F_L) , we further decompose it by using Shapley value (SV) based global sensitivity analysis to correctly quantify the contribution from each source of model uncertainty in Section 4.2. This information can provide a guide on which model F_ℓ to

collect more real-world data and improve the system mean performance estimation. Then, we provide the asymptotic consistency study over the variance component estimation for each source of uncertainty in Section 4.3.

4.1 Simulation and Model Uncertainty Contribution Quantification

Suppose that the parameters $(\tau^2, \boldsymbol{\theta}, C)$ are known, the simulation uncertainty can be characterized by a GP, and the simulation error follows a normal distribution. Then given the simulation outputs $\bar{\mathbf{Y}}_{\mathcal{D}}$, the simulation uncertainty is characterized by a GP, i.e., $M_p(\mathbf{x}) \sim \mathcal{N}(m_p(\mathbf{x}), \sigma_p^2(\mathbf{x}))$. Conditional on $\bar{\mathbf{Y}}_{\mathcal{D}}$, both $m_p(\mathbf{x})$ and $\sigma_p^2(\mathbf{x})$ are fixed functions. For notation simplification, all of following derivations are conditional on the simulation outputs $\bar{\mathbf{Y}}_{\mathcal{D}}$, but we will suppress the “ $|\bar{\mathbf{Y}}_{\mathcal{D}}$ ”.

To quantify the relative contribution of model and simulation uncertainties, we decompose the total variance of $M_p(\mathbf{X}_{\mathbf{m}})$ into two parts:

$$\begin{aligned}\sigma_T^2 &\equiv \text{Var}[M_p(\mathbf{X}_{\mathbf{m}})] \\ &= \text{E}\{\text{Var}[M_p(\mathbf{X}_{\mathbf{m}})|\mathbf{X}_{\mathbf{m}}]\} + \text{Var}\{\text{E}[M_p(\mathbf{X}_{\mathbf{m}})|\mathbf{X}_{\mathbf{m}}]\} \\ &= \text{E}[\sigma_p^2(\mathbf{X}_{\mathbf{m}})] + \text{Var}[m_p(\mathbf{X}_{\mathbf{m}})].\end{aligned}\quad (10)$$

The term $\sigma_M^2 \equiv \text{E}[\sigma_p^2(\mathbf{X}_{\mathbf{m}})]$ is a measure of the simulation uncertainty: the expected metamodel variance weighted by the density of moment estimator $\mathbf{X}_{\mathbf{m}}$. This weighting makes sense because the accuracy of the metamodel in regions with higher density is more important for the estimation of system mean performance. The term $\sigma_I^2 \equiv \text{Var}[m_p(\mathbf{X}_{\mathbf{m}})]$ is a measure of model uncertainty when we replace the unknown true response surface $\mu(\cdot)$ with its best linear unbiased estimate $m_p(\cdot)$.

If the simulation uncertainty disappears (i.e., $\sigma_p^2(\cdot) = 0$), then $\sigma_M^2 = 0$, CI_0 and CI_+ coincide. On the other hand, as $m \rightarrow \infty$ (more and more real-world data), $\mathbf{X}_{\mathbf{m}} \xrightarrow{a.s.} \mathbf{x}_c$ and since $m_p(\mathbf{x})$ is continuous we have $\sigma_I^2 = 0$; therefore, the width of CI_0 shrinks to zero as does coverage since there is remaining simulation uncertainty in general. However, because CI_+ accounts for simulation uncertainty it still provides asymptotically consistent coverage. This effect is demonstrated by the empirical study in Section 5.

Our decomposition allows us to express the total variance in Equation (10) as the sum of two variances measuring model and simulation uncertainties: $\sigma_T^2 = \sigma_I^2 + \sigma_M^2$. In the metamodel-assisted bootstrapping framework, we can estimate each variance component as follows:

- Total variance: $\hat{\sigma}_T^2 = \sum_{b=1}^B (M_b - \bar{M})^2 / (B - 1)$, where $\bar{M} = \sum_{b=1}^B M_b / B$.
- Model variance: $\hat{\sigma}_I^2 = \sum_{b=1}^B (\mu_b - \bar{\mu})^2 / (B - 1)$, where $\bar{\mu} = \sum_{b=1}^B \mu_b / B$.
- Simulation variance: $\hat{\sigma}_M^2 = \sum_{b=1}^B \sigma_p^2(\hat{\mathbf{X}}_{\mathbf{m}}^{(b)}) / B$.

The ratio $\hat{\sigma}_I / \hat{\sigma}_T$ provides an estimate of the relative contribution from model uncertainty on CI_+ . If it is close to 1, the contribution from simulation uncertainty can be ignored. Thus, this ratio can help a decision maker determine where to put more effort: If the model variance dominates, then get more real-world data (if possible). If the simulation variance dominates, then it can be reduced by more simulations, which can be a combination of additional design points and additional replications at existing design points. If neither dominates, then both activities are necessary to reduce CI_+ to a practically useful size.

4.2 Variance Decomposition for Model Uncertainty Analysis

The overall model variance $\sigma_I^2 = \text{Var}[m_p(\mathbf{X}_{\mathbf{m}})]$ is induced by the estimation uncertainty of correct moments $\mathbf{x}_c = (\mathbf{x}_{[1],c}, \mathbf{x}_{[2],c}, \dots, \mathbf{x}_{[L],c})$ for process models $F^c = \{F_1^c, F_2^c, \dots, F_L^c\}$. To efficiently identify the bottlenecks and reduce the impact of model uncertainty, we are interested in quantifying the contribution of moment estimation uncertainty of $\mathbf{X}_{\ell, m_\ell} = \mathbf{X}_\ell(\mathbf{Z}_{\ell, m_\ell})$ for each ℓ -th model F_ℓ . To approximate the estimation uncertainty of $\mathbf{X}_{\ell, m_\ell}$ with $\ell = 1, 2, \dots, L$, the bootstrap resampled moments are drawn from the bootstrap distribution, $\hat{\mathbf{X}}_{\ell, m_\ell} \sim F_{\mathbf{X}_{\ell, m_\ell}}(\cdot | \mathbf{Z}_{\ell, m_\ell}^{(0)})$.

Motivated by the SV based sensitivity analysis (see for example [31]), the overall model variance σ_I^2 in (10) can be decomposed as the sum of contributions from each source of model uncertainty,

$$\sigma_I^2 = \text{Var}[m_p(\mathbf{X}_{\mathbf{m}})] = \text{Var}[m_p(\mathbf{X}_{1, m_1}, \mathbf{X}_{2, m_2}, \dots, \mathbf{X}_{L, m_L})] = \sum_{\ell=1}^L s_\ell, \quad (11)$$

with s_ℓ quantifying the contribution from the ℓ -th model uncertainty,

$$s_\ell = \sum_{\mathcal{J} \subseteq \mathcal{L}/\{\ell\}} \frac{(L - |\mathcal{J}| - 1)! |\mathcal{J}|!}{L!} [c(\mathcal{J} \cup \{\ell\}) - c(\mathcal{J})], \quad (12)$$

where $\mathcal{L} = \{1, 2, \dots, L\}$ denotes the index set of L sources of model uncertainty and $|\cdot|$ indicates the set size. Here, for any subset $\mathcal{J} \subseteq \mathcal{L}$, we use the total effect based cost function $c(\mathcal{J}) = \mathbb{E}[\text{Var}[m_p(\mathbf{X}_m) | \mathbf{X}_{-\mathcal{J}}]]$ measuring the expected remaining variance when all other model moments, denoted by $\mathbf{X}_{-\mathcal{J}}$, are conditionally fixed, where $-\mathcal{J}$ denotes the remaining subset \mathcal{L}/\mathcal{J} .

The metamodel-assisted bootstrap resampling is used to estimate the contribution from each source of model uncertainty (Algorithm 1). Basically, for any model with the index $i \notin \mathcal{J}$ or $i \in \mathcal{L}/\mathcal{J}$, we take the sample moment $\mathbf{x}_{i, m_i}^{(0)}$ as true one. Denote these model moments by $\mathbf{x}_{-\mathcal{J}}^{(0)}$. Then, for the model with index $j \in \mathcal{J}$, we draw with replacement to generate the bootstrap sample moments quantifying the corresponding model uncertainty, $\widehat{\mathbf{X}}_{j, m_j}^{(b)} \sim F_{\mathbf{X}_{j, m_j}}(\cdot | \mathbf{z}_{j, m_j}^{(0)})$ with $b = 1, 2, \dots, B'$. We represent the combination of bootstrap moment samples for all model moments with index $j \in \mathcal{J}$ by $\widehat{\mathbf{X}}_{\mathcal{J}}^{(b)}$. Thus, we estimate $c(\mathcal{J})$ by a Monte Carlo sampling approach,

$$\widehat{c}(\mathcal{J}) = \frac{1}{B' - 1} \sum_{b=1}^{B'} \left[\widehat{m}_p(\mathbf{x}_{-\mathcal{J}}^{(0)}, \widehat{\mathbf{X}}_{\mathcal{J}}^{(b)}) - \bar{m}_{\mathcal{J}} \right]^2 \quad (13)$$

where $\bar{m}_{\mathcal{J}} = \sum_{b=1}^{B'} \widehat{m}_p(\mathbf{x}_{-\mathcal{J}}^{(0)}, \widehat{\mathbf{X}}_{\mathcal{J}}^{(b)}) / B'$. By plugging $\widehat{c}(\mathcal{J})$ into Equation (12), we can get the estimator \widehat{s}_ℓ quantifying the contribution from the ℓ -th model uncertainty to $\text{Var}[m_p(\mathbf{X}_m)]$. An efficient approximation algorithm, using the randomly selected subset instead of all possible index sets permutations, can be used to reduce the computational burden; see [31].

4.3 Asymptotic Consistency Study of Variance Contribution Estimation

We provide the asymptotic consistency study of variance contribution estimation from each source of uncertainty; see Theorems 4.1, 4.2, and 4.3.

Theorem 4.1. *Suppose that Assumptions 1–4 in Appendix A hold. Then conditional on $\bar{\mathbf{Y}}_{\mathcal{D}}$, the variance component estimators $\widehat{\sigma}_M^2, \widehat{\sigma}_I^2, \widehat{\sigma}_T^2$ are consistent as $m, B \rightarrow \infty$, where as $m \rightarrow \infty$ we have $m_\ell/m \rightarrow c_\ell$, $\ell = 1, 2, \dots, L$, for a constant $c_\ell > 0$. Specifically,*

- As $m \rightarrow \infty$, the model uncertainty disappears:

$$\lim_{m \rightarrow \infty} \sigma_M^2 = \sigma_p^2(\mathbf{x}_c), \quad \lim_{m \rightarrow \infty} \sigma_I^2 = 0 \quad \text{and} \quad \lim_{m \rightarrow \infty} \sigma_T^2 = \sigma_p^2(\mathbf{x}_c).$$

- As $m \rightarrow \infty$ and $B \rightarrow \infty$ in an iterated limit, the variance component estimators are consistent:

$$\begin{aligned} \lim_{m \rightarrow \infty} \lim_{B \rightarrow \infty} \widehat{\sigma}_M^2 &= \lim_{m \rightarrow \infty} \sigma_M^2 = \sigma_p^2(\mathbf{x}_c), \\ \lim_{m \rightarrow \infty} \lim_{B \rightarrow \infty} \widehat{\sigma}_I^2 &= \lim_{m \rightarrow \infty} \sigma_I^2 = 0, \\ \lim_{m \rightarrow \infty} \lim_{B \rightarrow \infty} \widehat{\sigma}_T^2 &= \lim_{m \rightarrow \infty} \sigma_T^2 = \sigma_p^2(\mathbf{x}_c), \\ \lim_{m \rightarrow \infty} \lim_{B \rightarrow \infty} \widehat{s}_\ell &= \lim_{m \rightarrow \infty} s_\ell = 0 \quad \text{for } \ell = 1, 2, \dots, L. \end{aligned}$$

Theorem 4.1 demonstrates that the variance components estimators $\widehat{\sigma}_I^2, \widehat{\sigma}_M^2, \widehat{\sigma}_T^2$, and \widehat{s}_ℓ for $\ell = 1, 2, \dots, L$ are consistent. However, we can see that the model uncertainty disappears as $m \rightarrow \infty$. In addition, we study the consistency of scaled versions of σ_I^2 and $\widehat{\sigma}_I^2$ in Theorem 4.2, showing that $m\sigma_I^2$ and $m\widehat{\sigma}_I^2$ converge to the same non-zero constant.

Theorem 4.2. *Suppose Assumptions 1–6 in Appendix A hold. Then we have $\lim_{m \rightarrow \infty} m\sigma_I^2 = \lim_{m \rightarrow \infty} \lim_{B \rightarrow \infty} m\widehat{\sigma}_I^2 = \sigma_\mu^2$ almost surely, where σ_μ^2 is a positive constant.*

Theorem 4.3. *Suppose Assumptions 1–6 in Appendix A hold. Then we have $\lim_{m \rightarrow \infty} m s_\ell = \lim_{m \rightarrow \infty} \lim_{B \rightarrow \infty} m\widehat{s}_\ell = \sigma_s^2$ almost surely, where σ_s^2 is a positive constant.*

Theorems 4.1–4.3 give the asymptotic properties of the variance component estimators, guaranteeing: (1) $\hat{\sigma}_I/\hat{\sigma}_T$ is a consistent estimator for the relative contribution of model uncertainty to the overall estimation uncertainty; and (2) \hat{s}_ℓ is a consistent estimator of the contribution from the ℓ -th model uncertainty. The detailed proof is provided in Appendix C. We will empirically evaluate its finite-sample performance in Section 5 where we form the variance component estimators by inserting $(\hat{\tau}^2, \hat{\boldsymbol{\theta}}, \hat{C})$ for the unknown parameters $(\tau^2, \boldsymbol{\theta}, C)$.

5 Empirical Study

We study the finite sample performance of the proposed metamodel-assisted uncertainty analysis framework and compare it with the direct bootstrap approach. We consider a biopharmaceutical manufacturing example in Sections 5.1. A cell culture process hybrid model for cell therapy manufacturing is studied in Section 5.2. Additionally, a queueing network example is provided in Appendix E. The proposed framework demonstrates good and robust performance under different experiment settings in terms of (1) the amount of real-world data m which controls the level of model uncertainty; (2) the simulation budget N which controls the simulation uncertainty; and (3) the number of design points k for GP metamodel construction, with N, k is used to control the metamodel uncertainty.

The empirical results show that the proposed framework can provide better performance than the direct bootstrap approach. The new ACI CI_+ is robust to different levels of real-world data m , number of design points k , and simulation budget N in terms of replications. When simulation uncertainty is significant, CI_0 tends to have undercoverage that becomes more serious as m increases. Since CI_+ accounts for both simulation and model uncertainties, it does not exhibit this degradation. The ratio $\hat{\sigma}_I/\hat{\sigma}_T$ is a useful measure of the relative contribution of model uncertainty to overall statistical uncertainty and the SV-based sensitivity analysis further quantifies the contribution from each source of model uncertainty.

5.1 A Biopharmaceutical Manufacturing Example

We consider the biomanufacturing example illustrated in Figure 1; see the details in [34]. We are interested in estimating the expected productivity of an antigen protein drug, i.e., $\mu(\mathbf{x}_c)$. The protein and impurity accumulations in the exponential-growth phase of fermentation process are modeled with the hybrid models, i.e., $X_t = X_0 \cdot e^{\gamma t} + \epsilon_P$ and $I_t = I_0 \cdot e^{\gamma t} + \epsilon_I$ with $0 \leq t \leq T$, where γ is the growth rate, X_0 and I_0 are the starting amounts of biomass and impurity. We consider the fixed harvest time $T = 54$ and the fixed initial impurity amount $I_0 = 14.64$.

The downstream purification process includes centrifuge, chromatography, filtration, and quality control. Random proportions of protein and impurity are removed at each operation unit, except at the quality control step. **(1) Centrifuge Step.** The protein and impurity levels before and after centrifuge are denoted by (X_F, I_F) and (X_C, I_C) . We assume that this step does not change the protein level, i.e., $X_C \equiv X_F$ [10], and it removes a random proportion of impurity, i.e., $I_C = Q \cdot I_F$. **(2) Chromatography Step.** For chromatography, random removal proportions of protein and impurity, denoted by Q_P and Q_I , follow uniform distributions [20]. The target protein and impurity levels before and after chromatography are denoted by (X_C, I_C) and (X_P, I_P) , and we have $X_P = Q_P \cdot X_C$ and $I_P = Q_I \cdot I_C$. **(3) Filtration Step.** Filtration works as a polishing procedure and it slightly reduces the impurity. Denote the protein and impurity levels before and after filtration with (X_P, I_P) and (X_{fr}, I_{fr}) . Thus, $I_{fr} = Q_{fr} \cdot I_P$. and $X_{fr} = X_P$. **(4) Quality Control Step.** During the quality control step, if the impurity percentage $\frac{I_{fr}}{X_{fr} + I_{fr}}$ is greater than the requirement, say $\omega = 25\%$, the corresponding batch is discarded. Therefore, the expected productivity of each batch is defined as:

$$\mu(\mathbf{x}_c) = \mathbb{E} \left[X_{fr} \cdot \mathbb{1} \left(\frac{I_{fr}}{X_{fr} + I_{fr}} \leq \omega \right) \right].$$

Table 1: The underlying true process model parameters.

	Protein Concentration	Impurity Concentration
Initial Biomass	$X_0 \sim \mathcal{N}(15.98, 4.17^2)$	N.A.
Growth Rate	$\gamma \sim \mathcal{N}(0.0475, 0.008^2)$	
Residual	$\epsilon_P \sim \mathcal{N}(0, 0.4918^2)$	$\epsilon_I \sim \mathcal{N}(0, 0.4918^2)$
Centrifuge	N.A.	$Q \sim \text{Unif}(0.4, 0.5)$
Chromatography	$Q_P \sim \text{Unif}(0.4833, 0.5907)$	$Q_I \sim \text{Unif}(0.1458, 0.1782)$
Filtration	N.A.	$Q_{fr} \sim \text{Unif}(0.99, 1)$

Thus, this biopharmaceutical manufacturing example has $L = 8$ process models: (1) F_1 modeling the residual or measurement error ϵ_P ; (2) F_2 modeling the batch-to-batch variation of the growth rate γ ; (3) F_3 modeling the variation

of the initial biomass X_0 ; (4) F_4 modeling the residual ϵ_I of impurity and metabolic waste accumulation; (5) F_5 modeling the random impurity removal ratio Q at centrifuge step; (6) F_6 and F_7 modeling the random removal ratios, Q_p and Q_I , of protein and impurity at chromatography step; and (7) F_8 modeling the random impurity removal ratio Q_{fr} at filtration step. All the underlying true model parameters are summarized in Table 1. In the empirical study, we assume that these parameters are unknown and they are estimated with finite observations with size m . Since we often have very limited biopharmaceutical manufacturing process data available in the real world, we focus on the cases with $m = 10, 20, 40$ and let $m_\ell = m$ for $\ell = 1, 2, \dots, L$.

We assess the performances of CI_+ and CI_0 especially under the situation when the system has large simulation uncertainty. Therefore, the run length for each replication is set as 2 after the warm up equal to 25 in terms of the number of batches. For the proposed metamodel-assisted uncertainty analysis framework, when we build the GP metamodel, we set the number of design points $k = 20, 40, 80$. The same number of replications is assigned to each design point, i.e., $n_j = n = N/k$ for $j = 1, 2, \dots, k$. To precisely estimate the percentile interval quantifying the system mean performance estimation uncertainty, we set the number of bootstrap resampled moments $B = 1000$ [3]. We compare the performance of our proposed framework with *direct bootstrap* under the same computational budget. In the direct bootstrap approach, we run simulations at each bootstrapped moments to estimate the system mean response and equally allocate the simulation budget. It means that the number of replications at each bootstrapped moment sample is $n^d = N/B$. To assess the coverage of CIs, we conduct a side experiment with 10^6 run length and 40 replications to estimate the true mean response and obtain $\mu(\mathbf{x}_c) = 116.759 \pm 0.006$.

5.1.1 Biomanufacturing System Uncertainty Quantification

Tables 2 and 3 show the mean and standard deviation (SD) results of width and coverage of 95% CIs, quantifying the overall estimation uncertainty of the expected productivity, obtained by the proposed metamodel-assisted uncertainty analysis framework and the direct bootstrap approach, when the simulation computational budget is $N = 2000, 4000$. We also record the ratio of model uncertainty to total variance $\hat{\sigma}_I^2/\hat{\sigma}_T^2$. All results are based on 500 macro-replications. As m increases, the contribution of model uncertainty, measured by $\hat{\sigma}_I^2/\hat{\sigma}_T^2$, decreases. The coverage of CI_+ is constantly better and closer to the nominal value of 95% compared with CI_0 . The direct bootstrap approach has substantial over coverage issue, which was described and explained in [4]. Since each experiment can be expensive and the average value of each batch of bio-drugs exceeds one million, this over coverage issue can lead to overly conservative decision making and dramatically impact the profit. Given the fixed computational budget, as the number of real-world data m increases, the mean and SD of the interval widths decrease, and the coverage becomes closer to the nominal value. *Overall, the proposed metamodel-assisted uncertainty analysis will provide better performance, especially under the situation with very limited amount of real-world data and high model uncertainty, which often happens in the biopharmaceutical manufacturing industry.*

Table 2: The CIs results (SD) of the expected productivity and $\hat{\sigma}_I^2/\hat{\sigma}_T^2$ when $N = 2000$.

$m = 10$	Metamodel-Assisted Uncertainty Analysis			Direct Bootstrap
	$k = 20, n=100$	$k = 40, n=50$	$k = 80, n=25$	
Coverage of CI_0	84.80%	88.20%	89.40%	99.60%
Coverage of CI_+	88.60%	90.40%	92.00%	
CI_0 Width	89.60 (32.99)	99.19 (37.08)	98.54 (33.62)	224.21
CI_+ Width	103.21 (35.81)	109.60 (38.66)	102.81 (35.09)	(81.25)
$\hat{\sigma}_I^2/\hat{\sigma}_T^2$	80.26%	88.99%	89.51%	61.10%
$m = 20$	Metamodel-Assisted Uncertainty Analysis			Direct Bootstrap
	$k = 20, n=100$	$k = 40, n=50$	$k = 80, n=25$	
Coverage of CI_0	85.80%	89.60%	89.60%	100.00%
Coverage of CI_+	92.60%	93.00%	92.60%	
CI_0 Width	64.09 (19.68)	66.98 (17.18)	70.96 (17.84)	205.85
CI_+ Width	75.46 (20.93)	74.69 (17.29)	79.01 (19.37)	(48.12)
$\hat{\sigma}_I^2/\hat{\sigma}_T^2$	76.55%	84.15%	83.62%	63.69%
$m = 40$	Metamodel-Assisted Uncertainty Analysis			Direct Bootstrap
	$k = 20, n=100$	$k = 40, n=50$	$k = 80, n=25$	
Coverage of CI_0	84.20%	91.00%	86.40%	100.00%
Coverage of CI_+	93.80%	95.40%	92.40%	
CI_0 Width	43.62 (11.38)	47.58 (10.26)	48.09 (10.42)	196.75
CI_+ Width	55.23 (12.59)	56.79 (10.86)	57.74 (11.73)	(32.74)
$\hat{\sigma}_I^2/\hat{\sigma}_T^2$	68.46%	74.73%	73.96%	65.03%

Table 3: The CIs results (SD) of the expected productivity and $\hat{\sigma}_I^2/\hat{\sigma}_T^2$ when $N = 4000$.

$m = 10$	Metamodel-Assisted Uncertainty Analysis			Direct Bootstrap
	$k = 20, n=200$	$k = 40, n=100$	$k = 80, n=50$	
Coverage of CI_0	86.80%	89.40%	91.20%	99.40%
Coverage of CI_+	91.20%	90.60%	92.80%	
CI_0 Width	91.96 (33.84)	103.24 (37.66)	99.45 (35.73)	178.19 (64.18)
CI_+ Width	102.84 (34.90)	108.23 (38.96)	103.46 (36.72)	
$\hat{\sigma}_I^2/\hat{\sigma}_T^2$	83.52%	92.78%	93.38%	72.20%
$m = 20$	Metamodel-Assisted Uncertainty Analysis			Direct Bootstrap
	$k = 20, n=200$	$k = 40, n=100$	$k = 80, n=50$	
Coverage of CI_0	88.80%	91.20%	91.60%	100.00%
Coverage of CI_+	92.40%	93.00%	93.40%	
CI_0 Width	65.58 (21.10)	69.49 (16.92)	73.37 (17.45)	156.94 (39.69)
CI_+ Width	75.87 (21.68)	74.64 (17.59)	78.50 (18.43)	
$\hat{\sigma}_I^2/\hat{\sigma}_T^2$	79.08%	88.86%	89.13%	75.56%
$m = 40$	Metamodel-Assisted Uncertainty Analysis			Direct Bootstrap
	$k = 20, n=200$	$k = 40, n=100$	$k = 80, n=50$	
Coverage of CI_0	87.00%	93.60%	91.60%	100.00%
Coverage of CI_+	94.80%	95.00%	94.80%	
CI_0 Width	45.69 (11.59)	49.66 (9.71)	51.19 (10.27)	145.75 (30.15)
CI_+ Width	54.52 (12.42)	55.87 (10.04)	57.18 (10.79)	
$\hat{\sigma}_I^2/\hat{\sigma}_T^2$	74.93%	82.37%	82.99%	77.71%

5.1.2 Biomanufacturing System Variance Decomposition

When the model uncertainty plays a dominate impact on the system performance estimation uncertainty, it is critical to identify the key source, which can be used to efficiently improve the simulation model. Based on the analytical study in Section 4.2, the means with 95% CI of the relative contribution from each ℓ -th model uncertainty, i.e., $(\hat{s}_\ell/\hat{\sigma}_I^2 \times 100\%)$, are recorded in Table 4. The results are estimated based on 100 macro-replications. We set the number of bootstrapped moments used for the variance estimation $B' = 2000$. Since the model uncertainty of protein generation process characterized by models for $\{\epsilon_P, \gamma, X_0\}$ dominates, we gradually increase m_ℓ with $\ell = 1, 2, 3$ as $m' = 10, 20, 40$, while fixing the number of real-world data for remaining models $m_\ell = 10$ for $\ell = 4, 5, \dots, L$. The order of importance, $\epsilon_P > \gamma > X_0$ is consistent across all sample sizes. Of the remaining variables, the removal proportion of protein at chromatography, Q_P , provides the largest proportion of contribution across all sample sizes and it increases dramatically as the sample size increases. As the sample size m' increases, the relative contribution from model uncertainty of $\{X_0, \gamma, \epsilon_P\}$ reduces. The overall model uncertainty, measured by σ_I , also decreases with increasing sample size.

This case study is motivated by a real animal bio-drug production. The quality requirement, i.e., $\frac{I_{fr}}{X_{fr}+I_{fr}} \leq \omega$ with $\omega = 25\%$, is relatively easy to meet through downstream purification. Thus, the results in Table 4 indicate that the influence of the impurity pathway parameters is negligible. This observation does not hold in general, especially for antigen proteins for human beings that typically have much more restrictive quality requirements (say $\omega = 1\%$).

Table 4: The relative contributions from each model uncertainty when $m' = 10, 20, 40$.

Process Model	$m'=10$	$m'=20$	$m'=40$
ϵ_P	44.51% \pm 5.05%	40.32% \pm 4.74%	37.73% \pm 4.53%
γ	35.18% \pm 4.93%	31.89% \pm 4.18%	28.44% \pm 3.69%
X_0	15.04% \pm 4.55%	14.34% \pm 4.28%	11.88% \pm 3.89%
Q_P	3.87% \pm 0.88%	10.44% \pm 2.16%	18.06% \pm 3.32%
ϵ_I	0.83% \pm 1.11%	1.90% \pm 1.81%	2.28% \pm 2.02%
Q	0.18% \pm 0.35%	0.33% \pm 0.53%	0.70% \pm 0.89%
Q_I	0.29% \pm 0.23%	0.35% \pm 0.37%	0.45% \pm 0.54%
Q_{fr}	0.04% \pm 0.12%	0.23% \pm 0.19%	0.64% \pm 0.94%
$\hat{\sigma}_I$	25.43 \pm 2.01	18.10 \pm 1.21	13.51 \pm 0.65

5.2 Cell Culture Expansion Scheduling for Cell Therapy Manufacturing

Here we use the erythroblast cell therapy manufacturing example presented in [12] to assess the performance of proposed framework. The cell culture of erythroblast exhibits two phases: a relatively uninhibited growth phase followed by an inhibited phase. The hybrid model cell growth and inhibitor accumulation is

$$\begin{aligned}\rho_{t+1} &= \rho_t + \Delta t \cdot r^g \rho_t \left(1 - \left(1 + e^{(k^s(k^c - I_t))} \right)^{-1} \right) + e_t^\rho, \\ I_{t+1} &= I_t + \Delta t \cdot \left(\frac{\rho_{t+1} - \rho_t}{\Delta t} - r^d I_t \right) + e_t^I,\end{aligned}$$

where Δt represents the time interval, ρ_t and I_t represent the cell density and the unobservable inhibitor concentration at the t -th time step. The kinetic coefficients r^g , k^s , k^c and r^d denote the cell growth rate, inhibitor sensitivity, inhibitor threshold, and inhibitor decay. The residuals follow the normal distributions, i.e., $e_t^\rho \sim N(0, (v^\rho)^2)$ and $e_t^I \sim N(0, (v^I)^2)$. There is raw material uncertainty for seed cell density, i.e., $\rho_0 \sim N(\mu_\rho, \sigma_\rho^2)$. The initial inhibitor concentration equals to 0 due to the fresh medium, i.e., $I_0 = 0$. Additionally, the investigation from [12] shows that the growth rate has significant variability cross different donors. Therefore, we incorporate batch-to-batch variation by considering the random effect on the growth rate, i.e., $r^g \sim \mathcal{N}(\mu^g, (\sigma^g)^2)$.

Thus, this erythroblast cell therapy manufacturing example has $L = 7$ process models: (1) F_1 for ρ_0 ; (2) F_2 for e^ρ ; (3) F_3 for e^I ; (4) F_4 for r^g ; and (5–7) the degenerate distributions F_5, F_6, F_7 for bioprocess kinetic parameters k^s, k^c, r^d . Set the underlying true parameters as $\{\mu_\rho, \sigma_\rho, v^\rho, v^I, \mu^g, \sigma^g\} = \{3, 0.03, 0.01, 0.01, 0.037, 0.008\}$ and $\{k^s, k^c, r^d\} = \{3.4, 2.6, 0.005\}$, which are validated by using the real-world data presented in [12]. In this empirical study, we assume that all these parameters are unknown and estimated with a finite amount of real-world data with size m . The cell density data are collected every 4 hours, i.e., $\Delta t = 4$ hours. Thus, we have m trajectory observations, i.e., $\boldsymbol{\tau}^{(i)} \equiv (\rho_0^{(i)}, \rho_1^{(i)}, \dots, \rho_T^{(i)})$ with $i = 1, 2, \dots, m$.

At any time t , if the batch-extension is performed, the original batch is scaled up to a λ times larger cell culture vessel filling with fresh medium. That means the cell density ρ and the concentration of inhibitor I decrease to $1/\lambda$ of original values. In this example, suppose that the batch-extension is scheduled at the 24-th hour (corresponding to time step $t = \frac{24}{\Delta t} + 1 = 7$). Then, the original batch is scaled up to $\lambda = 4$ fold. The cell culture process ends at $T = 40$ hours (corresponding to time step $t = \frac{T}{\Delta t} + 1 = 11$). Our goal is to estimate the expected productivity in terms of total biomass of target cells, i.e., $\mu(\mathbf{x}_c) = \mathbb{E}[\rho_T \cdot \lambda]$.

We focus on the cases with $m = 3, 6, 20$ and let $m_\ell = m$ for $\ell = 1, 2, \dots, L$. The total simulation budget is set to be $N = 4000$ replications. We compare the performance of our proposed framework with direct bootstrap approach under the same computational budget. For the proposed metamodel-assisted uncertainty analysis framework, we set the number of design points $k = 20, 40, 80$. The same number of replications is assigned to each design point, i.e., $n_j = n = N/k$ for $j = 1, 2, \dots, k$. The number of bootstrap resampled moments is set as $B = 1000$. In the direct bootstrap approach, the number of replications allocated at each bootstrapped moment sample is $n^d = N/B = 4$. To assess the coverage of CIs, we conduct a side experiment with 10^6 batches and 20 replications to estimate the true mean response and obtain $\mu(\mathbf{x}_c) = 17.32 \pm 0.004$.

Table 5 records the mean and standard deviation (SD) results of width and coverage of 95% CIs, quantifying the overall estimation uncertainty of the expected productivity, obtained by the proposed metamodel-assisted uncertainty analysis framework and the direct bootstrap approach. We also record the ratio of model uncertainty to total variance $\hat{\sigma}_I^2 / \hat{\sigma}_T^2$. All results are based on 500 macro-replications. The coverage of CI_+ is much closer to the nominal value of 95%, when compare with CI_0 . The direct bootstrap again exhibits overcoverage and provides much wider confidence interval width means and standard deviations. Given the fixed computational budget, as the number of real-world data m increases, the mean and SD of the interval widths decrease, and the coverage becomes closer to the nominal value.

6 Conclusions

To efficiently develop a simulation model to improve the assessment of the mean response for flexible and integrated biomanufacturing systems with modular design, we propose a metamodel-assisted bootstrapping uncertainty quantification and sensitivity analysis framework. Process model uncertainty is approximated by the bootstrap and an equation-based stochastic kriging metamodel is used to propagate the model uncertainty to the output mean. The simulation uncertainty is derived using properties of stochastic kriging. This framework delivers an interval quantifying the system mean response estimation accuracy accounting for both simulation and model uncertainties. The

Table 5: The CIs results (SD) of the expected productivity and $\widehat{\sigma}_I^2/\widehat{\sigma}_T^2$ when $N = 4000$.

$m = 3$	Metamodel-Assisted Uncertainty Analysis			Direct Bootstrap
	$k = 20, n=200$	$k = 40, n=100$	$k = 80, n=50$	
Coverage of CI_0	83.20%	86.20%	84.40%	99.80%
Coverage of CI_+	90.20%	91.20%	90.80%	
CI_0 Width	4.67 (2.11)	4.23 (2.42)	4.13 (2.45)	7.12
CI_+ Width	5.03 (2.75)	5.36 (2.76)	5.21 (2.52)	(3.75)
$\widehat{\sigma}_I^2/\widehat{\sigma}_T^2$	86.17%	90.23%	87.32%	87.21%
$m = 6$	Metamodel-Assisted Uncertainty Analysis			Direct Bootstrap
	$k = 20, n=100$	$k = 40, n=50$	$k = 80, n=25$	
Coverage of CI_0	89.60%	89.00%	89.20%	100.00%
Coverage of CI_+	92.80%	93.40%	91.60%	
CI_0 Width Mean	2.99 (1.86)	3.14 (1.76)	3.25 (1.78)	5.35
CI_+ Width Mean	3.34 (1.91)	3.42 (1.82)	3.43 (1.84)	(2.52)
$\widehat{\sigma}_I^2/\widehat{\sigma}_T^2$	86.34%	90.41%	91.02%	74.83%
$m = 20$	Metamodel-Assisted Uncertainty Analysis			Direct Bootstrap
	$k = 20, n=100$	$k = 40, n=50$	$k = 80, n=25$	
Coverage of CI_0	93.40%	94.00%	93.60%	97.80%
Coverage of CI_+	95.40%	95.00%	95.20%	
CI_0 Width Mean	1.68 (1.05)	1.72 (1.09)	1.74 (1.12)	3.84
CI_+ Width Mean	1.79 (1.10)	1.83 (1.12)	1.86 (1.15)	(1.72)
$\widehat{\sigma}_I^2/\widehat{\sigma}_T^2$	81.20%	85.16%	84.65%	80.14%

asymptotic consistency of this interval is proved under the assumption that the true response surface is a realization of a Gaussian process and certain parameters are known. Given very limited real-world observations and high stochastic uncertainty, the model uncertainty often dominates, especially for personalized bio-drug manufacturing. We provide a variance decomposition quantifying the relative contribution from each source of model uncertainty, as well as simulation uncertainty. While the asymptotic analysis shows correctness for the proposed framework, the empirical study on multiple biomanufacturing and service examples demonstrates that it also has good finite-sample performance.

Acknowledgments

This paper is based upon work supported by the National Science Foundation under Grant No. CMMI-0900354 and CMMI-1068473, National Institute of Standards and Technology (70NANB17H002), Department of Commerce. We also would like to thank the anonymous reviewers for their comments that have helped us improve the manuscript.

References

- [1] R. J. Adler. *The Geometry of Random Fields*. SIAM, Philadelphia, PA, 2010.
- [2] B. E. Ankenman, B. L. Nelson, and J. Staum. Stochastic kriging for simulation metamodeling. *Operations Research*, 58:371–382, 2010.
- [3] R. R. Barton, B. L. Nelson, and W. Xie. Quantifying input uncertainty via simulation confidence interval. *Informs Journal on Computing*, 26:74–87, 2014.
- [4] Russell R Barton et al. Presenting a more complete characterization of uncertainty: Can it be done. In *Proceedings of the 2007 INFORMS simulation society research workshop*, pages 26–60. INFORMS Simulation Society, 2007.
- [5] Russell R Barton and Lee W Schruben. Resampling methods for input modeling. In *Proceeding of the 2001 Winter Simulation Conference (Cat. No. 01CH37304)*, volume 1, pages 372–378. IEEE, 2001.
- [6] Bahar Biller and Canan G Corlu. Accounting for parameter uncertainty in large-scale stochastic simulations with correlated inputs. *Operations Research*, 59(3):661–673, 2011.
- [7] P. Billingsley. *Probability and Measure*. Wiley-Interscience, New York, 1995.
- [8] Emanuele Borgonovo and Elmar Plischke. Sensitivity analysis: a review of recent advances. *European Journal of Operational Research*, 248(3):869–887, 2016.
- [9] Canan G Corlu, Alp Akcay, and Wei Xie. Stochastic simulation under input uncertainty: A review. *Operations Research Perspectives*, page 100162, 2020.

- [10] M Delahaye, K Lawrence, SJ Ward, and M Hoare. An ultra scale-down analysis of the recovery by dead-end centrifugation of human cells for therapy. *Biotechnology and Bioengineering*, 112(5):997–1011, 2015.
- [11] Pauline M Doran. *Bioprocess Engineering Principles*. Academic Press, 2012.
- [12] Katie E Glen, Elizabeth A Cheeseman, Adrian J Stacey, and Robert J Thomas. A mechanistic model of erythroblast growth inhibition providing a framework for optimisation of cell therapy manufacturing. *Biochemical Engineering Journal*, 133:28–38, 2018.
- [13] Tanja Hernández Rodríguez, Christoph Posch, Julia Schmutzhard, Josef Stettner, Claus Weihs, Ralf Pörtner, and Björn Frahm. Predicting industrial-scale cell culture seed trains—a bayesian framework for model fitting and parameter estimation, dealing with uncertainty in measurements and model parameters, applied to a nonlinear kinetic cell culture model, using an mcmc method. *Biotechnology and Bioengineering*, 116(11):2944–2959, 2019.
- [14] D. Jones, M. Schonlau, and W Welch. Efficient global optimization of expensive black-box functions. *Journal of Global Optimization*, 13:455–492, 1998.
- [15] Jack PC Kleijnen. Regression and kriging metamodels with their experimental designs in simulation: a review. *European Journal of Operational Research*, 256(1):1–16, 2017.
- [16] Henry Lam and Huajie Qian. Subsampling variance for input uncertainty quantification. In *2018 Winter Simulation Conference (WSC)*, pages 1611–1622. IEEE, 2018.
- [17] Henry Lam and Huajie Qian. Subsampling to enhance efficiency in input uncertainty quantification. *Operations Research*, 70(3):1891–1913, 2022.
- [18] E.L. Lehmann and G. Casella. *Theory of Point Estimation*. Springer-Verlag, New York, 1998.
- [19] J. L. Loeppky, J. Sachs, and W. J Welch. Choosing the sample size of a computer experiment: A practical guide. *Technometrics*, 51:366–376, 2009.
- [20] Tugce Martagan, Ananth Krishnamurthy, Peter A Leland, and Christos T Maravelias. Performance guarantees and optimal purification decisions for engineered proteins. *Operations Research*, 66(1):18–41, 2017.
- [21] Linas Mockus, John J Peterson, Jose Miguel Lainez, and Gintaras V Reklaitis. Batch-to-batch variation: a key component for modeling chemical manufacturing processes. *Organic Process Research & Development*, 19(8):908–914, 2015.
- [22] Johannes Möller, Tanja Hernández Rodríguez, Jan Müller, Lukas Arndt, Kim B Kuchemüller, Björn Frahm, Regine Eibl, Dieter Eibl, and Ralf Pörtner. Model uncertainty-based evaluation of process strategies during scale-up of biopharmaceutical processes. *Computers & Chemical Engineering*, 134:106693, 2020.
- [23] Conor M. O’Brien, Qi Zhang, Prodromos Daoutidis, and Wei-Shou Hu. A hybrid mechanistic-empirical model for in silico mammalian cell bioprocess simulation. *Metabolic Engineering*, 66:31–40, 2021.
- [24] V. Picheny, D. Ginsbourger, O. Roustant, R. T. Haftka, and N. Kim. Adaptive designs of experiments for accurate approximation of a target region. *Journal of Mechanical Design*, 132:071008, 2010.
- [25] Tanja Hernández Rodríguez and Björn Frahm. Digital seed train twins and statistical methods. *Advances in Biochemical Engineering and Biotechnology*, 176:97–131, 2021.
- [26] T. J. Santner, B. J. Williams, and W. I. Notz. *The Design and Analysis of Computer Experiments*. Springer, New York, 2003.
- [27] R. J. Serfling. *Approximation Theorems of Mathematical Statistics*. Wiley, New York, 2002.
- [28] T.A. Severini. *Elements of Distribution Theory*. Cambridge University Press, New York, 2005.
- [29] J. Shao and D. Tu. *The Jackknife and Bootstrap*. Springer, New York, 1995.
- [30] Eunhye Song and Barry L Nelson. A quicker assessment of input uncertainty. In *2013 Winter Simulations Conference (WSC)*, pages 474–485. IEEE, 2013.
- [31] Eunhye Song, Barry L Nelson, and Jeremy Staum. Shapley effects for global sensitivity analysis: Theory and computation. *SIAM/ASA Journal on Uncertainty Quantification*, 4(1):1060–1083, 2016.
- [32] H. Sun and M. Farooq. Note on the generation of random points uniformly distributed in hyper-ellipsoids. In *Proceedings of the Fifth International Conference on Information Fusion*, pages 489–496, 2002.
- [33] A. W. Van Der Vaart. *Asymptotic Statistics*. Cambridge University Press, Cambridge, UK, 1998.
- [34] Bo Wang, Wei Xie, Tugce Martagan, Alp Akcay, and Canan G Corlu. Stochastic simulation model development for biopharmaceutical production process risk analysis and stability control. In *2019 Winter Simulation Conference (WSC)*, pages 1989–2000. IEEE, 2019.

- [35] Peng Wang, Lyudmila Mihaylova, Rohit Chakraborty, Said Munir, Martin Mayfield, Khan Alam, Muhammad Fahim Khokhar, Zhengkai Zheng, Chengxi Jiang, and Hui Fang. A gaussian process method with uncertainty quantification for air quality monitoring. *Atmosphere*, 12(1344):18, 2021.
- [36] W. Xie, B. L. Nelson, and J. Staum. The influence of correlation functions on stochastic kriging metamodels. In *2010 Winter Simulation Conference (WSC)*, pages 1067–1078. IEEE, 2010.
- [37] Wei Xie, Cheng Li, and Pu Zhang. A factor-based bayesian framework for risk analysis in stochastic simulations. *ACM Transactions on Modeling and Computer Simulation (TOMACS)*, 27(4):1–31, 2017.
- [38] Wei Xie, Bo Wang, Cheng Li, Dongming Xie, and Jared Auclair. Interpretable biomanufacturing process risk and sensitivity analyses for quality-by-design and stability control. *Naval Research Logistics (NRL)*, 69(3):461–483, 2022.
- [39] Wei Xie, Bo Wang, and Qiong Zhang. Metamodel-assisted risk analysis for stochastic simulation with input uncertainty. In *2018 Winter Simulation Conference (WSC)*, pages 1766–1777. IEEE, 2018.
- [40] Qiong Zhang, Bo Wang, and Wei Xie. A pooled percentile estimator for parallel simulations. *Journal of Simulation*, 16(1):73–83, 2022.
- [41] F. Zouaoui and J. R. Wilson. Accounting for parameter uncertainty in simulation input modeling. *IIE Transactions*, 35:781–792, 2003.
- [42] F. Zouaoui and J. R. Wilson. Accounting for input-model and input-parameter uncertainties in simulation. *IIE Transactions*, 36:1135–1151, 2004.

Appendix

In this appendix we prove Theorems 3.1, 4.1–4.3 and provide a brief description of the experiment design used to build stochastic kriging metamodels. We also use a queue network example to illustrate the proposed framework is general even though it is motivated by the critical needs from biopharmaceutical manufacturing industry.

To be self-contained, we first state some definitions, lemmas and theorems that are used in the proofs. Let \xrightarrow{D} denote convergence in distribution.

- **Borel-Cantelli Lemma** [7]: For events A_1, A_2, \dots , if $\sum_{n=1}^{\infty} \Pr(A_n)$ converges, then

$$\Pr\left(\limsup_n A_n\right) = 0$$

where

$$\limsup_n A_n = \bigcap_{n=1}^{\infty} \bigcup_{k=n}^{\infty} A_k$$

is the set of outcomes that occur infinitely many times.

- **Lemma 2.11** [33]: Suppose that $\mathbf{X}_n \xrightarrow{D} \mathbf{X}$ for a random vector \mathbf{X} with a continuous distribution function. Then the distribution function of \mathbf{X}_n converges uniformly to that of \mathbf{X} : $\|F_{\mathbf{X}_n} - F_{\mathbf{X}}\|_{\infty} \rightarrow 0$, where $\|h\|_{\infty}$ is the sup-norm of h on \mathfrak{R} , $\|h\|_{\infty} = \sup_t |h(t)|$.
- **Portmanteau Lemma** [33]: For any random vectors \mathbf{X}_n and \mathbf{X} the following statements are equivalent.
 1. $\mathbf{X}_n \xrightarrow{D} \mathbf{X}$.
 2. $E[f(\mathbf{X}_n)] \rightarrow E[f(\mathbf{X})]$ for all bounded, continuous functions f .
- **Theorem 2.3** [33]: Let $g : \mathfrak{R}^k \rightarrow \mathfrak{R}^m$ be continuous at every point in a set \mathcal{C} such that $\Pr\{X \in \mathcal{C}\} = 1$. Then
 1. If $X_n \xrightarrow{D} X$ then $g(X_n) \xrightarrow{D} g(X)$.
 2. If $X_n \xrightarrow{P} X$ then $g(X_n) \xrightarrow{P} g(X)$.
 3. If $X_n \xrightarrow{a.s.} X$ then $g(X_n) \xrightarrow{a.s.} g(X)$.

In the proofs when we refer to the “continuous mapping theorem” we will mean Theorem 2.3.

- **Glivenko-Cantelli Theorem** [33]: If X_1, X_2, \dots, X_n are i.i.d. random variables with distribution function F and F_n is the empirical cdf of X_1, X_2, \dots, X_n , then $\|F_n - F\|_{\infty} \xrightarrow{a.s.} 0$ as $n \rightarrow \infty$.

- **Lemma 21.2** [33]: For cdf F , define the inverse cdf to be

$$F^{-1}(p) = \inf\{t: F(t) \geq p\}.$$

Then a sequence of cdfs $F_n(t) \rightarrow F(t)$ for every t where F is continuous if and only if $F_n^{-1}(p) \rightarrow F^{-1}(p)$ for every p where F^{-1} is continuous.

- **Theorem 13.1** [28]: Let $\mathbf{X}_1, \mathbf{X}_2, \dots$ denote a sequence of d -dimensional random vectors such that, for some vector $\boldsymbol{\mu}$,

$$\sqrt{n}(\mathbf{X}_n - \boldsymbol{\mu}) \xrightarrow{D} N(\mathbf{0}_{d \times 1}, \Sigma) \text{ as } n \rightarrow \infty,$$

where Σ is a $d \times d$ positive definite matrix with $|\Sigma| < \infty$. Let $g: \mathbb{R}^d \rightarrow \mathbb{R}^k$ denote a continuously differentiable function and let $\nabla g(\mathbf{x})$ denote the $d \times k$ matrix of partial derivatives of g with respect to \mathbf{x} . Then

$$\sqrt{n}(g(\mathbf{X}_n) - g(\boldsymbol{\mu})) \xrightarrow{D} N(\mathbf{0}_{k \times 1}, \nabla g(\boldsymbol{\mu})^\top \Sigma \nabla g(\boldsymbol{\mu})) \text{ as } n \rightarrow \infty.$$

- **Theorem 3.8** [29]: Let $\mathbf{X}_1, \mathbf{X}_2, \dots, \mathbf{X}_m$ denote d -dimensional i.i.d. random vectors and $\bar{\mathbf{X}}_m = m^{-1} \sum_{i=1}^m \mathbf{X}_i$. Let $\bar{\mathbf{X}}_m^* = m^{-1} \sum_{i=1}^m \mathbf{X}_i^*$ where $\{\mathbf{X}_1^*, \mathbf{X}_2^*, \dots, \mathbf{X}_m^*\}$ are randomly and independently drawn with replacement from $\{\mathbf{X}_1, \mathbf{X}_2, \dots, \mathbf{X}_m\}$. Let $g: \mathbb{R}^d \rightarrow \mathbb{R}^k$ denote a continuously differentiable function and $\nabla g(\mathbf{x})$ denote the $d \times k$ matrix of partial derivatives of g with respect to \mathbf{x} . Let $T_m = g(\bar{\mathbf{X}}_m)$ and denote the bootstrap variance estimator for T_m by $v_m^* = \text{Var}_*[g(\bar{\mathbf{X}}_m^*)]$.

Suppose that $E[\mathbf{X}_1^\top \mathbf{X}_1] < \infty$ and $\nabla g(\boldsymbol{\mu}) \neq \mathbf{0}_{d \times k}$ where $\boldsymbol{\mu} = E[\mathbf{X}_1]$. Suppose further that

$$\max_{i_1, \dots, i_m} |T_m(\mathbf{X}_{i_1}, \dots, \mathbf{X}_{i_m}) - T_m| / \tau_m \xrightarrow{a.s.} 0, \quad (14)$$

where the maximum is taken over all integers i_1, \dots, i_m satisfying $1 \leq i_1 \leq \dots \leq i_m \leq m$, and $\{\tau_m\}$ is a sequence of positive numbers satisfying $\liminf_m \tau_m > 0$ and $\tau_m = O(e^{m^q})$ with a $q \in (0, 1/2)$. Then v_m^* is strongly consistent, i.e., $v_m^* / \sigma_m^2 \xrightarrow{a.s.} 1$, where $\sigma_m^2 = m^{-1} \nabla g(\boldsymbol{\mu})^\top \Sigma \nabla g(\boldsymbol{\mu})$ and $\Sigma = \text{Var}(\mathbf{X}_1)$.

- **Theorem 1.1** ([18], Chapter 6): Let X_1, X_2, \dots, X_m be i.i.d. with $E(X_1) = \mu$, $\text{Var}(X_1) = \sigma^2$, and finite fourth moment, and suppose h is a function of a real variable whose first four derivatives $h'(x), h''(x), h^{(3)}(x)$ and $h^{(4)}(x)$ exist for all $x \in I$, where I is an interval with $\Pr(X_1 \in I) = 1$. Furthermore, suppose that $|h^{(4)}(x)| \leq M$ for all $x \in I$, for some $M < \infty$. Then

$$E[h(\bar{X})] = h(\mu) + \frac{\sigma^2}{2m} h''(\mu) + \mathcal{R}_m.$$

If, in addition, the fourth derivative of h^2 is also bounded, then

$$\text{Var}[h(\bar{X})] = \frac{\sigma^2}{m} [h'(\mu)]^2 + \mathcal{R}_m.$$

In both cases the remainder \mathcal{R}_m is $O(1/m^2)$.

- **Multivariate Taylor Formula** ([27], page 44): Let the function g defined on \mathbb{R}^d possess continuous partial derivatives of order n at each point of an open set $S \subset \mathbb{R}^d$. Let $\mathbf{x} \in S$. For each point \mathbf{y} , $\mathbf{y} \neq \mathbf{x}$, such that the line segment $L(\mathbf{x}, \mathbf{y})$ joining \mathbf{x} and \mathbf{y} lies in S , there exists a point \mathbf{z} in the interior of $L(\mathbf{x}, \mathbf{y})$ such that

$$\begin{aligned} g(\mathbf{y}) &= g(\mathbf{x}) + \sum_{k=1}^{n-1} \frac{1}{k!} \sum_{i_1=1}^d \dots \sum_{i_k=1}^d \frac{\partial^k g(t_1, \dots, t_d)}{\partial t_{i_1} \dots \partial t_{i_k}} \Bigg|_{\mathbf{t}=\mathbf{x}} \cdot \prod_{j=1}^k (y_{i_j} - x_{i_j}) \\ &+ \frac{1}{n!} \sum_{i_1=1}^d \dots \sum_{i_n=1}^d \frac{\partial^n g(t_1, \dots, t_d)}{\partial t_{i_1} \dots \partial t_{i_n}} \Bigg|_{\mathbf{t}=\mathbf{z}} \cdot \prod_{j=1}^n (y_{i_j} - x_{i_j}). \end{aligned}$$

A Assumptions for Asymptotic Study

Assumptions that are needed for the asymptotic analysis of interval CI_+ and variance decomposition are summarized below. Assumptions 1–2 give sufficient conditions for the almost sure (a.s.) consistency of bootstrap moment estimators $\hat{\mathbf{X}}_m \xrightarrow{a.s.} \mathbf{x}_c$ as $m \rightarrow \infty$ (see Lemma 1 in B). Under Assumption 3, a GP $M(\cdot)$ with a correlation function satisfying Condition (15) has continuous sample paths almost surely; see [1] Theorem 3.4.1. Condition (15) is satisfied by many correlation functions used in practice, and in particular any power exponential correlation function

$r(\mathbf{x} - \mathbf{x}') = \exp(-\sum_{j=1}^d \theta_j |x_j - x'_j|^p)$ with $0 < p \leq 2$ and $\theta_j > 0$ [26]. Assumption 4 indicates that process data are collected independently of the simulation model, and that our uncertainty about the mean response surface as represented by $M(\mathbf{x})$ is independent of the stochastic simulation noise (although both can depend on \mathbf{x}). Assumptions 5–6 are for the asymptotic consistency study of variance component estimators $\hat{\sigma}_I^2$ and $\hat{\sigma}_\ell^2$.

Assumptions (★):

1. The ℓ th model distribution is uniquely determined by its first h_ℓ moments and it has finite first $4h_\ell$ moments for $\ell = 1, 2, \dots, L$.
2. We have i.i.d observations $Z_{\ell,1}^{(0)}, Z_{\ell,2}^{(0)}, \dots, Z_{\ell,m_\ell}^{(0)}$ from the ℓ th distribution for $\ell = 1, 2, \dots, L$. As $m \rightarrow \infty$, we have $m_\ell/m \rightarrow c_\ell$, $\ell = 1, 2, \dots, L$, for a constant $c_\ell > 0$.
3. The $\epsilon_j(\mathbf{x}) \stackrel{i.i.d.}{\sim} \mathbf{N}(0, \sigma_\epsilon^2(\mathbf{x}))$ for any \mathbf{x} , and $M(\mathbf{x})$ is a stationary, separable GP with a continuous correlation function satisfying

$$1 - r(\mathbf{x} - \mathbf{x}') \leq \frac{c}{|\log(\|\mathbf{x} - \mathbf{x}'\|_2)|^{1+\gamma}} \text{ for all } \|\mathbf{x} - \mathbf{x}'\|_2 \leq \delta \quad (15)$$

for some $c > 0$, $\gamma > 0$ and $\delta < 1$, where $\|\mathbf{x} - \mathbf{x}'\|_2 = \sqrt{\sum_{j=1}^d (x_j - x'_j)^2}$.

4. Process observations $Z_{\ell j}^{(0)}$, simulation noise $\epsilon_j(\mathbf{x})$ and GP $M(\mathbf{x})$ are mutually independent. The bootstrap process is independent of all of them.
5. The first three derivatives of the correlation function of the GP $M(\mathbf{x})$ exist and the third derivative is bounded.
6. $m_\ell/m \rightarrow 1$ for $\ell = 1, 2, \dots, L$.

B Asymptotic Consistency of CI₊

To prove Theorem 1, we first establish three supporting lemmas.

Lemma 1. Suppose that Assumptions 1–2 hold. Then the bootstrap resampled moments converge almost surely to the true moments $\widehat{\mathbf{X}}_m \xrightarrow{a.s.} \mathbf{x}_c$ as $m \rightarrow \infty$.

Proof: Since all of the input processes are independent, we establish the result for one input distribution F^c without loss of generality. We prove the result for \mathbf{x}_c being the generic h th-order moment, $\alpha_h \equiv \mathbb{E}(Z^h) < \infty$, for $Z \sim F^c$.

The h th-order bootstrap resampled moment is

$$\widehat{X}_m = \frac{1}{m} \sum_{j=1}^m (Z^{(j;m)})^h \text{ with } Z^{(j;m)} \stackrel{i.i.d.}{\sim} \mathbf{Z}_m^{(0)} \quad (16)$$

where “ $Z^{(j;m)} \sim \mathbf{Z}_m^{(0)}$ ” denotes the j th independent sample with replacement from $\mathbf{Z}_m^{(0)}$. We use the Chebychev Inequality and the Borel-Cantelli Lemma to prove the result.

By the Chebychev Inequality, for every $\epsilon > 0$, we have

$$\Pr \left\{ |\widehat{X}_m - \alpha_h| > \epsilon \right\} \leq \frac{\mathbb{E} \left[(\widehat{X}_m - \alpha_h)^4 \right]}{\epsilon^4}. \quad (17)$$

Notice that

$$\mathbb{E} \left[(\widehat{X}_m - \alpha_h)^4 \right] = \mathbb{E} \left[\widehat{X}_m^4 \right] - 4\alpha_h \mathbb{E} \left[\widehat{X}_m^3 \right] + 6\alpha_h^2 \mathbb{E} \left[\widehat{X}_m^2 \right] - 4\alpha_h^3 \mathbb{E} \left[\widehat{X}_m \right] + \alpha_h^4. \quad (18)$$

We will analyze each term in Equation (18). First, we show that any i th bootstrap resampled moment, denoted as $\widehat{\alpha}_i$, is unbiased,

$$\begin{aligned} \mathbb{E} [\widehat{\alpha}_i] &\equiv \mathbb{E} \left[\frac{1}{m} \sum_{j=1}^m (Z^{(j;m)})^i \right] \\ &= \mathbb{E} \left[\mathbb{E} \left[(Z^{(j;m)})^i \mid Z_1^{(0)}, \dots, Z_m^{(0)} \right] \right] \end{aligned} \quad (19)$$

$$\begin{aligned}
&= \mathbf{E} \left[\frac{1}{m} \sum_{j=1}^m (Z_j^{(0)})^i \right] \\
&= \alpha_i.
\end{aligned}$$

Thus, $\mathbf{E}[\widehat{X}_m] = \alpha_h$. Notice that

$$\begin{aligned}
\mathbf{E}[\widehat{X}_m^2] &= \mathbf{E} \left[\left(\frac{1}{m} \sum_{j=1}^m (Z^{(j;m)})^h \right)^2 \right] \\
&= \frac{1}{m^2} \mathbf{E} \left[\left(\sum_{j=1}^m (Z^{(j;m)})^h \right)^2 \right] \\
&= \frac{1}{m^2} \mathbf{E} \left[\sum_{j=1}^m (Z^{(j;m)})^{2h} + \sum_{i \neq j} (Z^{(i;m)})^h (Z^{(j;m)})^h \right] \\
&= \frac{1}{m^2} (m\alpha_{2h} + m(m-1) \\
&\quad \cdot \mathbf{E} \left[\mathbf{E}[(Z^{(i;m)})^h | Z_1^{(0)}, \dots, Z_m^{(0)}] \cdot \mathbf{E}[(Z^{(j;m)})^h | Z_1^{(0)}, \dots, Z_m^{(0)}] \right]) \\
&= \frac{1}{m^2} \left(m\alpha_{2h} + m(m-1) \mathbf{E} \left[\left(\frac{1}{m} \sum_{i=1}^m (Z_i^{(0)})^h \right)^2 \right] \right) \\
&= \frac{1}{m^2} \left(m\alpha_{2h} + \frac{m(m-1)}{m^2} \mathbf{E} \left[\sum_{i=1}^m (Z_i^{(0)})^{2h} + \sum_{i \neq j} (Z_i^{(0)})^h (Z_j^{(0)})^h \right] \right) \\
&= \frac{1}{m^2} \left(m\alpha_{2h} + \frac{m(m-1)}{m^2} (m\alpha_{2h} + m(m-1)\alpha_h^2) \right) \\
&= \frac{1}{m^2} [(2m-1)\alpha_{2h} + (m-1)^2\alpha_h^2] \\
&= \frac{2}{m}\alpha_{2h} + \left(1 - \frac{2}{m}\right)\alpha_h^2 + O(m^{-2})
\end{aligned}$$

where $O(m^{-2})$ means terms at most order $1/m^2$. Similar derivations show that

$$\begin{aligned}
\mathbf{E}[\widehat{X}_m^3] &= \frac{1}{m^4} ([m(4m-3) + (m-1)(m-2)]\alpha_{3h} \\
&\quad + [3m(m-1)^2 + 3(m-1)^2(m-2)]\alpha_h\alpha_{2h} + (m-1)^2(m-2)^2\alpha_h^3) \\
&= \frac{6}{m}\alpha_h\alpha_{2h} + \left(1 - \frac{6}{m}\right)\alpha_h^3 + O(m^{-2})
\end{aligned}$$

and

$$\mathbf{E}[\widehat{X}_m^4] = \frac{12}{m}\alpha_h^2\alpha_{2h} + \left(1 - \frac{12}{m}\right)\alpha_h^4 + O(m^{-2}).$$

Thus,

$$\begin{aligned}
\mathbf{E}[(\widehat{X}_m - \alpha_h)^4] &= \mathbf{E}[\widehat{X}_m^4] - 4\alpha_h\mathbf{E}[\widehat{X}_m^3] + 6\alpha_h^2\mathbf{E}[\widehat{X}_m^2] - 4\alpha_h^3\mathbf{E}[\widehat{X}_m] + \alpha_h^4 \tag{20} \\
&= \frac{12}{m}\alpha_h^2\alpha_{2h} + \left(1 - \frac{12}{m}\right)\alpha_h^4 - 4\alpha_h \left[\frac{6}{m}\alpha_h\alpha_{2h} + \left(1 - \frac{6}{m}\right)\alpha_h^3 \right] \\
&\quad + 6\alpha_h^2 \left[\frac{2}{m}\alpha_{2h} + \left(1 - \frac{2}{m}\right)\alpha_h^2 \right] - 3\alpha_h^4 + O(m^{-2}) \\
&= 0 + O(m^{-2})
\end{aligned}$$

because all of the $O(m^{-1})$ terms cancel. Therefore, combining Equations (17), (18) and (20), we have

$$\sum_{m=1}^{\infty} \Pr\{|\hat{X}_m - \alpha_h| > \epsilon\} \leq \sum_{m=1}^{\infty} \frac{c}{m^2 \epsilon^4} < \infty$$

where c is some finite constant. Thus, if $\alpha_{4h} < \infty$, then $\hat{X}_m \xrightarrow{a.s.} \alpha_h$ by the first Borel-Cantelli Lemma in Section 4 of [7].

Since Assumption 2 guarantees $m_\ell \rightarrow \infty$ for each moment associated with the ℓ th model, we can generalize the almost sure convergence to a vector of moments by applying the converging together lemma. Therefore, we have $\hat{\mathbf{X}}_m \xrightarrow{a.s.} \mathbf{x}_c$. \square

Remark: The independent variables in our stochastic kriging metamodel consist of central moments and standardized central moments. Since standardized moments are continuous functions of raw moments, we can use the continuous mapping theorem to obtain corresponding almost sure convergence of the standardized moments.

Given a fixed and finite number of design points $\mathbf{x}_1, \mathbf{x}_2, \dots, \mathbf{x}_k$, let $\mathbf{M} = (M(\mathbf{x}_1), M(\mathbf{x}_2), \dots, M(\mathbf{x}_k))^\top$. The simulation error at design point \mathbf{x}_i is $\epsilon(\mathbf{x}_i)$, so let $\bar{\epsilon}(\mathbf{x}_i) = \sum_{j=1}^{n_i} \epsilon(\mathbf{x}_i) / n_i$ for $i = 1, 2, \dots, k$ denote the average. Therefore, the sample means of simulation outputs at all design points can be represented as $\bar{\mathbf{Y}}_D = \mathbf{M} + \bar{\epsilon}$, where $\bar{\epsilon} = (\bar{\epsilon}(\mathbf{x}_1), \bar{\epsilon}(\mathbf{x}_2), \dots, \bar{\epsilon}(\mathbf{x}_k))^\top$. Finally, let $M_p(\cdot)$ be a GP having the conditional distribution of $M(\cdot)$ given $\bar{\mathbf{Y}}_D$.

Lemma 2. Suppose Assumptions 3–4 hold. Then $M_p(\cdot)$ has continuous sample paths almost surely.

Proof: Let (Ω_M, P_M) be the underlying probability space for the GP $M(\cdot)$, and $(\Omega_\epsilon, P_\epsilon)$ be the underlying probability space for $\bar{\epsilon}$. Notice that $(\Omega_\epsilon, P_\epsilon)$ depends on the particular design points $\mathbf{x}_1, \mathbf{x}_2, \dots, \mathbf{x}_k$ and corresponding numbers of replications n_1, n_2, \dots, n_k which we consider fixed and given, while (Ω_M, P_M) does not.

Let $\omega_M \in \Omega_M$ be an elementary outcome and $M(\cdot, \omega_M)$ the resulting random function. For notational convenience, let $\mathbf{M}(\omega_M) = (M(\mathbf{x}_1, \omega_M), M(\mathbf{x}_2, \omega_M), \dots, M(\mathbf{x}_k, \omega_M))^\top$ the random function evaluated at $\mathbf{x}_1, \mathbf{x}_2, \dots, \mathbf{x}_k$. Similarly, $\bar{\epsilon} = \bar{\epsilon}(\omega_\epsilon)$ for elementary outcome $\omega_\epsilon \in \Omega_\epsilon$. Notice that under Assumption 3, $\bar{\epsilon}(\omega_\epsilon)$ has a multivariate normal distribution.

Theorem 3.4.1 of [1] asserts that there is a P_M -measurable set $\Omega_M^c \subset \Omega_M$ such that $\Pr\{\omega_M \in \Omega_M^c\} = P_M(\Omega_M^c) = 1$, and for every $\omega_M \in \Omega_M^c$ the function $M(\cdot, \omega_M)$ is continuous.

The random variable $\bar{\mathbf{Y}}_D$ maps $\Omega = \Omega_M \times \Omega_\epsilon \rightarrow \mathfrak{R}^k$ as $\bar{\mathbf{Y}}_D(\omega) = \mathbf{M}(\omega_M) + \bar{\epsilon}(\omega_\epsilon)$ for $\omega = (\omega_M, \omega_\epsilon) \in \Omega$ with probability measure $P = P_M \cdot P_\epsilon$ since they are independent. Our goal is to prove that

$$\Pr\{\omega_M \in \bar{\Omega}_M^c | \bar{\mathbf{Y}}_D\} = 0 \tag{21}$$

almost surely.

We know that $0 \leq \Pr\{\omega_M \in \bar{\Omega}_M^c | \bar{\mathbf{Y}}_D\} \leq 1$ with probability 1. But also

$$0 = \Pr\{\omega_M \in \bar{\Omega}_M^c\} = \mathbb{E} [\Pr\{\omega_M \in \bar{\Omega}_M^c | \bar{\mathbf{Y}}_D\}].$$

Therefore, (21) must hold. \square

Lemma 3. Suppose that Assumptions 1–4 hold. Then $M_p(\hat{\mathbf{X}}_m) \xrightarrow{a.s.} M_p(\mathbf{x}_c)$ as $m \rightarrow \infty$.

Proof: Under Assumption 3, the GP $M(\cdot)$ has continuous sample paths almost surely; applying Lemma 2, $M_p(\cdot)$ also has continuous sample paths almost surely. Under Assumptions 1–2, $\hat{\mathbf{X}}_m \xrightarrow{a.s.} \mathbf{x}_c$ as $m \rightarrow \infty$ by Lemma 1. And $M_p(\cdot)$ and $\hat{\mathbf{X}}_m$ are independent. The result follows by applying the continuous mapping theorem. \square

Theorem 3.1. Suppose that Assumptions 1–4 hold. Then the interval $[M_{(\lceil B \frac{\alpha}{2} \rceil)}, M_{(\lceil B(1-\frac{\alpha}{2}) \rceil)}]$ is asymptotically consistent, meaning

$$\lim_{m \rightarrow \infty} \lim_{B \rightarrow \infty} \Pr\{M_{(\lceil B \alpha / 2 \rceil)} \leq M_p(\mathbf{x}_c) \leq M_{(\lceil B(1-\alpha/2) \rceil)}\} = 1 - \alpha. \tag{22}$$

Proof: Define $K_{\mathbf{m}}(t) \equiv \Pr \left\{ M_p(\widehat{\mathbf{X}}_{\mathbf{m}}) \leq t \right\}$. Notice that the distribution $K_{\mathbf{m}}(t)$ depends on both the distributions of $M_p(\cdot)$ and $\widehat{\mathbf{X}}_{\mathbf{m}}$. Specifically,

$$\begin{aligned} K_{\mathbf{m}}(t) &= \int \Pr \left\{ M_p(\mathbf{x}) \leq t \mid \widehat{\mathbf{X}}_{\mathbf{m}} = \mathbf{x} \right\} d\widehat{F}_{\mathbf{X}_{\mathbf{m}}}(\mathbf{x} \mid \mathbf{z}_{\mathbf{m}}^{(0)}) \\ &= \int \Phi \left(\frac{t - m_p(\mathbf{x})}{\sigma_p(\mathbf{x})} \right) d\widehat{F}_{\mathbf{X}_{\mathbf{m}}}(\mathbf{x} \mid \mathbf{z}_{\mathbf{m}}^{(0)}). \end{aligned}$$

Thus, $K_{\mathbf{m}}(t)$ is a continuous distribution almost surely. Let $\widehat{K}_{\mathbf{m}}$ be the empirical cdf of M_1, M_2, \dots, M_B , which are i.i.d. from $K_{\mathbf{m}}(t)$. Notice that $\widehat{K}_{\mathbf{m}}^{-1}(\gamma) = M_{(\lceil B\gamma \rceil)}$ for $\gamma = \alpha/2$ and $1 - \alpha/2$.

By the Glivenko-Cantelli Theorem [33], $\|K_{\mathbf{m}} - \widehat{K}_{\mathbf{m}}\|_{\infty} \xrightarrow{a.s.} 0$ as $B \rightarrow \infty$. Therefore, by Lemma 21.2 of [33],

$$|M_{(\lceil B\gamma \rceil)} - K_{\mathbf{m}}^{-1}(\gamma)| \xrightarrow{a.s.} 0$$

as $B \rightarrow \infty$ for $\gamma = \alpha/2, 1 - \alpha/2$. As a result,

$$\begin{aligned} &\lim_{B \rightarrow \infty} \Pr \{ M_{(\lceil B\alpha/2 \rceil)} \leq M_p(\mathbf{x}_c) \leq M_{(\lceil B(1-\alpha/2) \rceil)} \} \\ &= \Pr \{ K_{\mathbf{m}}^{-1}(\alpha/2) \leq M_p(\mathbf{x}_c) \leq K_{\mathbf{m}}^{-1}(1 - \alpha/2) \}. \end{aligned}$$

Therefore, Equation (22) becomes

$$\lim_{m \rightarrow \infty} \Pr \{ K_{\mathbf{m}}^{-1}(\alpha/2) \leq M_p(\mathbf{x}_c) \leq K_{\mathbf{m}}^{-1}(1 - \alpha/2) \} = 1 - \alpha. \quad (23)$$

To show Equation (23), we only need to show that

$$\lim_{m \rightarrow \infty} \Pr \{ K_{\mathbf{m}}^{-1}(\alpha/2) > M_p(\mathbf{x}_c) \} = \alpha/2$$

because the proof of the upper bound is similar.

Since, conditional on $\bar{\mathbf{Y}}_{\mathcal{D}}$, $M_p(\mathbf{x}_c) \sim \mathcal{N}(m_p(\mathbf{x}_c), \sigma_p^2(\mathbf{x}_c))$, the cdf $H(t) \equiv \Pr \{ M_p(\mathbf{x}_c) \leq t \}$ is continuous. By Lemma 3 and Lemma 2.11 in [33],

$$\begin{aligned} &\sup_t |\Pr \{ M_p(\widehat{\mathbf{X}}_{\mathbf{m}}) \leq t \} - \Pr \{ M_p(\mathbf{x}_c) \leq t \}| \\ &= \|K_{\mathbf{m}} - H\|_{\infty} \rightarrow 0 \text{ as } m \rightarrow \infty. \end{aligned}$$

Therefore,

$$\begin{aligned} &\Pr \{ K_{\mathbf{m}}^{-1}(\alpha/2) > M_p(\mathbf{x}_c) \} \\ &= \Pr \{ \alpha/2 \geq K_{\mathbf{m}}(M_p(\mathbf{x}_c)) \} \\ &= \Pr \{ \alpha/2 \geq H(M_p(\mathbf{x}_c)) \} + o(1) \\ &= \Pr \{ M_p(\mathbf{x}_c) \leq H^{-1}(\alpha/2) \} + o(1) \\ &= \alpha/2 + o(1). \end{aligned} \quad (24)$$

Equation (24) is obtained because

$$|K_{\mathbf{m}}(M_p(\mathbf{x}_c)) - H(M_p(\mathbf{x}_c))| \leq \|K_{\mathbf{m}} - H\|_{\infty} \rightarrow 0 \text{ as } m \rightarrow \infty.$$

Thus, we have

$$\begin{aligned} &\lim_{m \rightarrow \infty} \Pr \{ K_{\mathbf{m}}^{-1}(\alpha/2) \leq M_p(\mathbf{x}_c) \leq K_{\mathbf{m}}^{-1}(1 - \alpha/2) \} \\ &= \lim_{m \rightarrow \infty} \Pr \{ M_p(\mathbf{x}_c) \leq K_{\mathbf{m}}^{-1}(1 - \alpha/2) \} - \lim_{m \rightarrow \infty} \Pr \{ M_p(\mathbf{x}_c) < K_{\mathbf{m}}^{-1}(\alpha/2) \} \\ &= (1 - \alpha/2) - \alpha/2 \\ &= 1 - \alpha. \end{aligned}$$

□

C Asymptotic Analysis of Variance Contribution Estimation

Theorem 4.1. Suppose that Assumptions 1–4 hold. Then the variance component estimators $\hat{\sigma}_M^2$, $\hat{\sigma}_I^2$, $\hat{\sigma}_T^2$, and \hat{s}_ℓ for $\ell = 1, 2, \dots, L$ are consistent as $m, B \rightarrow \infty$.

Proof: When a GP $M(\cdot)$ has a continuous correlation function with all parameters finite, the SK predictor

$$m_p(\mathbf{x}) = \hat{\beta}_0 + \tau^2 R(\mathbf{x})^\top [\Sigma + C]^{-1} (\bar{\mathbf{Y}}_{\mathcal{D}} - \hat{\beta}_0 \cdot \mathbf{1}_{k \times 1}), \quad (25)$$

and corresponding variance

$$\sigma_p^2(\mathbf{x}) = \tau^2 - \tau^4 R(\mathbf{x})^\top [\Sigma + C]^{-1} R(\mathbf{x}) + \eta^\top [1_{k \times 1}^\top (\Sigma + C)^{-1} 1_{k \times 1}]^{-1} \eta$$

where $R(\mathbf{x})^\top = (r(\mathbf{x} - \mathbf{x}_1), r(\mathbf{x} - \mathbf{x}_2), \dots, r(\mathbf{x} - \mathbf{x}_k))$ and $\eta = 1 - 1_{k \times 1}^\top (\Sigma + C)^{-1} \tau^2 R(\mathbf{x})$, are continuous and bounded functions of \mathbf{x} .

By the Strong Law of Large Numbers, the raw moment estimator $\mathbf{X}_m \xrightarrow{a.s.} \mathbf{x}_c$ as $m \rightarrow \infty$ under Assumptions 1–2. This almost sure convergence can be extended to central moments and standardized central moments by the continuous mapping theorem. By applying the Portmanteau Lemma in [33], we have

$$\lim_{m \rightarrow \infty} \sigma_M^2 = \lim_{m \rightarrow \infty} \int \sigma_p^2(\mathbf{x}) dF_{\mathbf{X}_m}^c(\mathbf{x}) = \lim_{m \rightarrow \infty} \mathbb{E}[\sigma_p^2(\mathbf{X}_m)] = \sigma_p^2(\mathbf{x}_c),$$

and

$$\begin{aligned} \lim_{m \rightarrow \infty} \sigma_I^2 &= \lim_{m \rightarrow \infty} \int (m_p(\mathbf{x}) - \mu_0)^2 dF_{\mathbf{X}_m}^c(\mathbf{x}) \\ &= \lim_{m \rightarrow \infty} \mathbb{E} \left[(m_p(\mathbf{X}_m) - \mathbb{E}[m_p(\mathbf{X}_m)])^2 \right] \\ &= (m_p(\mathbf{x}_c) - m_p(\mathbf{x}_c))^2 = 0 \end{aligned}$$

where $\mu_0 = \int \int \nu dF(\nu|\mathbf{x}) dF_{\mathbf{X}_m}^c(\mathbf{x}) = \int m_p(\mathbf{x}) dF_{\mathbf{X}_m}^c(\mathbf{x})$.

Recall that $F(\nu|\mathbf{x})$ is a normal distribution $\mathcal{N}(m_p(\mathbf{x}), \sigma_p^2(\mathbf{x}))$. Let $g(\mathbf{x}) \equiv \int (\nu - \mu_0)^2 dF(\nu|\mathbf{x})$. Then

$$\begin{aligned} \lim_{m \rightarrow \infty} \sigma_T^2 &= \lim_{m \rightarrow \infty} \int \int (\nu - \mu_0)^2 dF(\nu|\mathbf{x}) dF_{\mathbf{X}_m}^c(\mathbf{x}) \\ &= \lim_{m \rightarrow \infty} \int g(\mathbf{x}) dF_{\mathbf{X}_m}^c(\mathbf{x}). \end{aligned}$$

However,

$$\begin{aligned} g(\mathbf{x}) &= \int (\nu - m_p(\mathbf{x}) + m_p(\mathbf{x}) - \mu_0)^2 dF(\nu|\mathbf{x}) \\ &= \int (\nu - m_p(\mathbf{x}))^2 dF(\nu|\mathbf{x}) + (m_p(\mathbf{x}) - \mu_0)^2 \\ &\quad + (m_p(\mathbf{x}) - \mu_0) \int (\nu - m_p(\mathbf{x})) dF(\nu|\mathbf{x}) \\ &= \sigma_p^2(\mathbf{x}) + (m_p(\mathbf{x}) - \mu_0)^2 + 0. \end{aligned}$$

Since $m_p(\mathbf{x})$ and $\sigma_p^2(\mathbf{x})$ are continuous and bounded functions, so is $g(\mathbf{x})$. Therefore,

$$\lim_{m \rightarrow \infty} \sigma_T^2 = \lim_{m \rightarrow \infty} \mathbb{E}[g(\mathbf{X}_m)] = g(\mathbf{x}_c) = \sigma_p^2(\mathbf{x}_c)$$

by applying the Portmanteau Lemma.

Next, we will show consistency of the variance estimators. By Lemma 1, $\hat{\mathbf{X}}_m \xrightarrow{a.s.} \mathbf{x}_c$. For the metamodel uncertainty estimator, we have

$$\lim_{m \rightarrow \infty} \lim_{B \rightarrow \infty} \hat{\sigma}_M^2 = \lim_{m \rightarrow \infty} \lim_{B \rightarrow \infty} \frac{1}{B} \sum_{b=1}^B \sigma_p^2(\hat{\mathbf{X}}_m^{(b)})$$

$$\begin{aligned}
&= \lim_{m \rightarrow \infty} \mathbb{E} \left[\sigma_p^2(\widehat{\mathbf{X}}_{\mathbf{m}}) | \mathbf{Z}_{\mathbf{m}}^{(0)} \right] \\
&= \sigma_p^2(\mathbf{x}_c).
\end{aligned}$$

The last step follows by applying the Portmanteau Lemma.

For the input uncertainty estimator, we have

$$\begin{aligned}
\lim_{m \rightarrow \infty} \lim_{B \rightarrow \infty} \widehat{\sigma}_I^2 &= \lim_{m \rightarrow \infty} \lim_{B \rightarrow \infty} \frac{B}{B-1} \left[\frac{1}{B} \sum_{b=1}^B m_p^2(\widehat{\mathbf{X}}_{\mathbf{m}}^{(b)}) - \bar{\mu}^2 \right] \\
&= \lim_{m \rightarrow \infty} \left(\mathbb{E} \left[m_p^2(\widehat{\mathbf{X}}_{\mathbf{m}}) | \mathbf{Z}_{\mathbf{m}}^{(0)} \right] - \mathbb{E}^2 \left[m_p(\widehat{\mathbf{X}}_{\mathbf{m}}) | \mathbf{Z}_{\mathbf{m}}^{(0)} \right] \right) \\
&= m_p^2(\mathbf{x}_c) - m_p^2(\mathbf{x}_c) = 0.
\end{aligned}$$

The last step follows by applying Lemma 1 and the Portmanteau Lemma.

For the total variance estimator, we have

$$\begin{aligned}
\lim_{m \rightarrow \infty} \lim_{B \rightarrow \infty} \widehat{\sigma}_T^2 &= \lim_{m \rightarrow \infty} \lim_{B \rightarrow \infty} \frac{B}{B-1} \left(\frac{1}{B} \sum_{b=1}^B M_b^2 - \bar{M}^2 \right) \\
&= \lim_{m \rightarrow \infty} \mathbb{E} \left[M_p^2(\widehat{\mathbf{X}}_{\mathbf{m}}) | \mathbf{Z}_{\mathbf{m}}^{(0)} \right] - \lim_{m \rightarrow \infty} \mathbb{E}^2 \left[M_p(\widehat{\mathbf{X}}_{\mathbf{m}}) | \mathbf{Z}_{\mathbf{m}}^{(0)} \right] \\
&= \mathbb{E} \left[M_p^2(\mathbf{x}_c) \right] - \mathbb{E}^2 \left[M_p(\mathbf{x}_c) \right] \\
&= m_p^2(\mathbf{x}_c) + \sigma_p^2(\mathbf{x}_c) - m_p^2(\mathbf{x}_c) \\
&= \sigma_p^2(\mathbf{x}_c).
\end{aligned} \tag{26}$$

By Lemma 3, $M_p(\widehat{\mathbf{X}}_{\mathbf{m}}) \xrightarrow{a.s.} M_p(\mathbf{x}_c)$ as $m \rightarrow \infty$. Then Step (26) follows by applying Portmanteau Lemma.

To show the consistency of \widehat{s}_ℓ for $\ell = 1, 2, \dots, L$, we first study the cost function $\widehat{c}(\mathcal{J})$ and show it converges for any set \mathcal{J} ,

$$\begin{aligned}
\lim_{m \rightarrow \infty} \lim_{B \rightarrow \infty} \widehat{c}(\mathcal{J}) &= \lim_{m \rightarrow \infty} \lim_{B \rightarrow \infty} \frac{1}{B-1} \sum_{b=1}^B \left[m_p \left(\mathbf{x}_{-\mathcal{J}}^{(0)}, \widehat{\mathbf{X}}_{\mathcal{J}}^{(b)} \right) - \bar{m}_{\mathcal{J}} \right]^2 \\
&= \lim_{m \rightarrow \infty} \lim_{B \rightarrow \infty} \frac{B}{B-1} \left[\frac{1}{B} \sum_{b=1}^B m_p^2 \left(\mathbf{x}_{-\mathcal{J}}^{(0)}, \widehat{\mathbf{X}}_{\mathcal{J}}^{(b)} \right) - \bar{m}_{\mathcal{J}}^2 \right] \\
&= \lim_{m \rightarrow \infty} \left(\mathbb{E} \left[m_p^2 \left(\mathbf{x}_{-\mathcal{J}}^{(0)}, \widehat{\mathbf{X}}_{\mathcal{J}} \right) | \mathbf{Z}_{\mathbf{m}}^{(0)} \right] - \mathbb{E}^2 \left[m_p \left(\mathbf{x}_{-\mathcal{J}}^{(0)}, \widehat{\mathbf{X}}_{\mathcal{J}} \right) | \mathbf{Z}_{\mathbf{m}}^{(0)} \right] \right) \\
&\stackrel{(*)}{=} m_p^2(\mathbf{x}_c) - m_p^2(\mathbf{x}_c) = 0.
\end{aligned} \tag{27}$$

Step (*) follows by applying Lemma 1 and the Portmanteau Lemma. Then, for the Shapley Value based variance estimator, we can show

$$\begin{aligned}
\lim_{m \rightarrow \infty} \lim_{B \rightarrow \infty} \widehat{s}_\ell &= \lim_{m \rightarrow \infty} \lim_{B \rightarrow \infty} \sum_{\mathcal{J} \subset \mathcal{L} \setminus \{\ell\}} \frac{(L - |\mathcal{J}| - 1)! |\mathcal{J}|!}{L!} [\widehat{c}(\mathcal{J} \cup \{\ell\}) - \widehat{c}(\mathcal{J})] \\
&= \sum_{\mathcal{J} \subset \mathcal{L} \setminus \{\ell\}} \frac{(L - |\mathcal{J}| - 1)! |\mathcal{J}|!}{L!} \left[\lim_{m \rightarrow \infty} \lim_{B \rightarrow \infty} \widehat{c}(\mathcal{J} \cup \{\ell\}) - \lim_{m \rightarrow \infty} \lim_{B \rightarrow \infty} \widehat{c}(\mathcal{J}) \right] \\
&= 0.
\end{aligned}$$

For the finite number of set \mathcal{J} , the last step follows by applying (27). \square

Theorem 4.2. Suppose that Assumptions 1–4 and the following additional assumptions hold:

5. The first three derivatives of the correlation function of the GP $M(\mathbf{x})$ exist and the third derivative is bounded; and

6. $m_\ell/m \rightarrow 1$ for $\ell = 1, 2, \dots, L$.

Then $\lim_{m \rightarrow \infty} m\sigma_I^2 = \lim_{m \rightarrow \infty} \lim_{B \rightarrow \infty} m\widehat{\sigma}_I^2 = \sigma_\mu^2$ almost surely, where σ_μ^2 is a positive constant.

Proof: Under Assumptions 1–2, and applying the multivariate central limit theorem, we have as $m \rightarrow \infty$,

$$\sqrt{m}(\mathbf{X}_m - \mathbf{x}_c) \xrightarrow{D} \mathbf{N}(\mathbf{0}_{d \times 1}, \Lambda)$$

where Λ denotes the $d \times d$ positive definite asymptotic variance-covariance matrix of \mathbf{X}_m .

When a GP $M(\mathbf{x})$ has a continuous correlation function with all parameters finite, the SK predictor

$$m_p(\mathbf{x}) = \widehat{\beta}_0 + \tau^2 R(\mathbf{x})^\top [\Sigma + C]^{-1} (\bar{\mathbf{Y}}_{\mathcal{D}} - \widehat{\beta}_0 \cdot \mathbf{1}_{k \times 1}), \quad (28)$$

given the simulation sample mean $\bar{\mathbf{Y}}_{\mathcal{D}}$, is continuous and bounded. Under Assumption 5, the gradient $\nabla m_p(\mathbf{x})$ exists and is continuous. We will show that $\nabla m_p(\mathbf{x}) \neq \mathbf{0}_{d \times 1}$ almost surely. By taking the derivative of $m_p(\mathbf{x})$ in Equation (28), we have

$$\frac{\partial m_p(\mathbf{x})}{\partial x_j} = \underbrace{\frac{\partial R(\mathbf{x})^\top}{\partial x_j}}_{\mathbf{A}} \tau^2 [\Sigma + C]^{-1} (\bar{\mathbf{Y}}_{\mathcal{D}} - \widehat{\beta}_0 \cdot \mathbf{1}_{k \times 1}). \quad (29)$$

Since $\partial R(\mathbf{x})^\top / \partial x_j = (\partial r(\mathbf{x} - \mathbf{x}_1) / \partial x_j, \partial r(\mathbf{x} - \mathbf{x}_2) / \partial x_j, \dots, \partial r(\mathbf{x} - \mathbf{x}_k) / \partial x_j) \neq \mathbf{0}_{1 \times k}$ and $\tau^2 [\Sigma + C]^{-1}$ is positive definite, \mathbf{A} is a non-zero constant vector. Under Assumption 3, $\mathbf{A}(\bar{\mathbf{Y}}_{\mathcal{D}} - \widehat{\beta}_0 \cdot \mathbf{1}_{k \times 1})$ is a normal random variable that is equal to 0 with probability 0. Thus, $\nabla m_p(\mathbf{x}) \neq \mathbf{0}_{d \times 1}$ almost surely. Applying Theorem 13.1 in [28], we have

$$\sqrt{m}(m_p(\mathbf{X}_m) - m_p(\mathbf{x}_c)) \xrightarrow{D} \mathbf{N}(0, \sigma_\mu^2)$$

where $\sigma_\mu^2 = \nabla m_p(\mathbf{x}_c)^\top \Lambda \nabla m_p(\mathbf{x}_c) > 0$. This establishes the constant.

Since $m_p(\cdot)$ is continuous and bounded, there always exists a finite $M_1 > 0$ such that $|m_p(\mathbf{x})| < M_1$ for all $\mathbf{x} \in \mathbb{R}^d$. Therefore, $\max_{\mathbf{x} \in \mathbb{R}^d} |m_p(\mathbf{x}) - m_p(\mathbf{X}_m)| < 2M_1$. Let $\tau_m = e^{m^{1/4}}$. Since $2M_1/\tau_m \rightarrow 0$ as $m \rightarrow \infty$, Condition (14) of Theorem 3.8 of [29] holds. Thus, the bootstrap variance estimator is strongly consistent: $\lim_{m \rightarrow \infty} \lim_{B \rightarrow \infty} m\widehat{\sigma}_I^2 = \sigma_\mu^2$ almost surely.

Next, we will show $\lim_{m \rightarrow \infty} m\sigma_I^2 = \sigma_\mu^2$ by proving a multi-variate version of Theorem 1.1 in [18], Chapter 6. Let $L(\mathbf{X}_m, \mathbf{x}_c)$ denote the line segment joining \mathbf{X}_m and \mathbf{x}_c . By the Multivariate Taylor Formula [27],

$$\begin{aligned} m_p(\mathbf{X}_m) &= m_p(\mathbf{x}_c) + \nabla m_p(\mathbf{x}_c)^\top (\mathbf{X}_m - \mathbf{x}_c) \\ &\quad + \frac{1}{2} (\mathbf{X}_m - \mathbf{x}_c)^\top \nabla^2 m_p(\mathbf{x}_c) (\mathbf{X}_m - \mathbf{x}_c) + \mathcal{R}(\mathbf{X}_m, \mathbf{x}_c). \end{aligned}$$

The remainder term

$$\mathcal{R}(\mathbf{X}_m, \mathbf{x}_c) = \frac{1}{3!} \sum_{i_1=1}^d \sum_{i_2=1}^d \sum_{i_3=1}^d \left. \frac{\partial^3 m_p(x_1, \dots, x_d)}{\partial x_{i_1} \partial x_{i_2} \partial x_{i_3}} \right|_{\mathbf{x}=\mathbf{z}} \prod_{j=1}^3 (X_{m,i_j} - x_{c,i_j})$$

where \mathbf{z} denotes a value in the interior of $L(\mathbf{X}_m, \mathbf{x}_c)$, and $X_{m,i}$ and $x_{c,i}$ denote the i th components of the vectors \mathbf{X}_m and \mathbf{x}_c . By taking the expectation over both sides, we have

$$\mathbb{E}[m_p(\mathbf{X}_m)] = m_p(\mathbf{x}_c) + \frac{1}{2} \mathbb{E}[(\mathbf{X}_m - \mathbf{x}_c)^\top \nabla^2 m_p(\mathbf{x}_c) (\mathbf{X}_m - \mathbf{x}_c)] + \mathbb{E}[\mathcal{R}(\mathbf{X}_m, \mathbf{x}_c)] \quad (30)$$

where ∇^2 is the Hessian operator.

We will show that the second and third terms on the RHS of Equation (30) are $O(m^{-1})$ and $O(m^{-2})$, respectively, under Assumption 5. Since all of the input processes are independent, we establish the result for one input distribution F^c without loss of generality.

We prove the result for \mathbf{x}_c being the generic h th-order moment, $x_{c,h} = \mathbb{E}(Z_1^h) < \infty$, and $X_{m,h} = m^{-1} \sum_{j=1}^m Z_j^h$ for $Z_j \stackrel{\text{iid}}{\sim} F^c$.

Let $C_{ij} \equiv \frac{1}{2} [\nabla^2 m_p(\mathbf{x}_c)]_{i,j}$. We first consider components of the second term on the RHS of Equation (30).

$$\mathbb{E}[C_{ij}(X_{m,i} - x_{c,i})(X_{m,j} - x_{c,j})]$$

$$\begin{aligned}
&= C_{ij} \mathbb{E} \left[\frac{1}{m} \sum_{k_1=1}^m (Z_{k_1}^i - x_{c,i}) \cdot \frac{1}{m} \sum_{k_2=1}^m (Z_{k_2}^j - x_{c,j}) \right] \\
&= \frac{C_{ij}}{m^2} \mathbb{E} \left[\sum_{k=1}^m (Z_k^i - x_{c,i})(Z_k^j - x_{c,j}) + \sum_{k_1 \neq k_2} (Z_{k_1}^i - x_{c,i})(Z_{k_2}^j - x_{c,j}) \right] \\
&= \frac{C_{ij}}{m^2} \mathbb{E} \left[\sum_{k=1}^m (Z_k^i - x_{c,i})(Z_k^j - x_{c,j}) + 0 \right] = O\left(\frac{1}{m}\right).
\end{aligned}$$

The last two steps follow because the Z_i are i.i.d. and Assumption 5 holds. Thus, the second term on the RHS of Equation (30) is

$$\begin{aligned}
&\frac{1}{2} \mathbb{E}[(\mathbf{X}_m - \mathbf{x}_c)^\top \nabla^2 m_p(\mathbf{x}_c) (\mathbf{X}_m - \mathbf{x}_c)] \\
&= \sum_{i=1}^d \sum_{j=1}^d \mathbb{E}[C_{ij} (X_{m,i} - x_{c,i})(X_{m,j} - x_{c,j})] = O\left(\frac{1}{m}\right).
\end{aligned}$$

Similarly, for the components of the third term of the RHS of Equation (30), we have

$$\begin{aligned}
&D_{ijk} \mathbb{E}[(X_{m,i} - x_{c,i})(X_{m,j} - x_{c,j})(X_{m,k} - x_{c,k})] \\
&= D_{ijk} \mathbb{E} \left[\frac{1}{m^3} \sum_{k_1=1}^m (Z_{k_1}^i - x_{c,i}) \cdot \sum_{k_2=1}^m (Z_{k_2}^j - x_{c,j}) \cdot \sum_{k_3=1}^m (Z_{k_3}^k - x_{c,k}) \right] \\
&= \frac{D_{ijk}}{m^3} \mathbb{E} \left[\sum_{k_1=1}^m (Z_{k_1}^i - x_{c,i})(Z_{k_1}^j - x_{c,j})(Z_{k_1}^k - x_{c,k}) + 0 \right] = O\left(\frac{1}{m^2}\right).
\end{aligned}$$

where

$$D_{ijk} \equiv \frac{1}{3!} \frac{\partial^3 m_p(x_1, \dots, x_d)}{\partial x_i \partial x_j \partial x_k} \Big|_{\mathbf{x}=\mathbf{z}}.$$

Again, the last two steps follow because the Z_i are i.i.d. and Assumption 5 holds. Thus, the third term in Equation (30) is

$$\begin{aligned}
&\mathbb{E}[\mathcal{R}(\mathbf{X}_m, \mathbf{x}_c)] \\
&= \sum_{i=1}^d \sum_{j=1}^d \sum_{k=1}^d D_{ijk} \mathbb{E}[(X_{m,i} - x_{c,i})(X_{m,j} - x_{c,j})(X_{m,k} - x_{c,k})] = O\left(\frac{1}{m^2}\right).
\end{aligned}$$

Squaring both sides of Equation (30), we have

$$[\mathbb{E}(m_p(\mathbf{X}_m))]^2 = m_p^2(\mathbf{x}_c) + m_p(\mathbf{x}_c) \mathbb{E}[(\mathbf{X}_m - \mathbf{x}_c)^\top \nabla^2 m_p(\mathbf{x}_c) (\mathbf{X}_m - \mathbf{x}_c)] + O\left(\frac{1}{m^2}\right). \quad (31)$$

By repeating the same derivation that results in Equation (30) but using $m_p^2(\cdot)$ instead of $m_p(\cdot)$, we obtain

$$\begin{aligned}
\mathbb{E}[m_p^2(\mathbf{X}_m)] &= m_p^2(\mathbf{x}_c) + \frac{1}{2} \mathbb{E}[(\mathbf{X}_m - \mathbf{x}_c)^\top \nabla^2 m_p^2(\mathbf{x}_c) (\mathbf{X}_m - \mathbf{x}_c)] + O\left(\frac{1}{m^2}\right) \\
&= m_p^2(\mathbf{x}_c) + \mathbb{E} \left[(\mathbf{X}_m - \mathbf{x}_c)^\top \nabla m_p(\mathbf{x}_c) \nabla m_p(\mathbf{x}_c)^\top (\mathbf{X}_m - \mathbf{x}_c) \right. \\
&\quad \left. + (\mathbf{X}_m - \mathbf{x}_c)^\top m_p(\mathbf{x}_c) \nabla^2 m_p(\mathbf{x}_c) (\mathbf{X}_m - \mathbf{x}_c) \right] + O\left(\frac{1}{m^2}\right). \quad (32)
\end{aligned}$$

Then,

$$\begin{aligned}
\text{Var}[m_p(\mathbf{X}_m)] &= \mathbb{E}[m_p^2(\mathbf{X}_m)] - (\mathbb{E}[m_p(\mathbf{X}_m)])^2 \\
&= \mathbb{E}[(\mathbf{X}_m - \mathbf{x}_c)^\top \nabla m_p(\mathbf{x}_c) \nabla m_p(\mathbf{x}_c)^\top (\mathbf{X}_m - \mathbf{x}_c)] + O\left(\frac{1}{m^2}\right)
\end{aligned}$$

$$\begin{aligned}
&= \mathbb{E}[\nabla m_p(\mathbf{x}_c)^\top (\mathbf{X}_m - \mathbf{x}_c)(\mathbf{X}_m - \mathbf{x}_c)^\top \nabla m_p(\mathbf{x}_c)] + O\left(\frac{1}{m^2}\right) \\
&= \frac{1}{m} \nabla m_p(\mathbf{x}_c)^\top \Lambda \nabla m_p(\mathbf{x}_c) + O\left(\frac{1}{m^2}\right).
\end{aligned} \tag{33}$$

Step (33) follows because $\nabla m_p(\mathbf{x}_c)^\top (\mathbf{X}_m - \mathbf{x}_c)$ is a scalar. Thus, we have $\lim_{m \rightarrow \infty} m\sigma_I^2 = \sigma_\mu^2$. \square

Theorem 4.3. Suppose that Assumptions 1–6 hold. Then $\lim_{m \rightarrow \infty} ms_\ell = \lim_{m \rightarrow \infty} \lim_{B \rightarrow \infty} m\widehat{s}_\ell = \sigma_s^2$ almost surely, where σ_s^2 is a positive constant.

Proof:

Following the continuous mapping theorem, we have:

$$\begin{aligned}
\lim_{m \rightarrow \infty} \lim_{B \rightarrow \infty} m\widehat{s}_\ell &= \lim_{m \rightarrow \infty} \lim_{B \rightarrow \infty} m \sum_{\mathcal{J} \subset \mathcal{L}/\{\ell\}} \frac{(L - |\mathcal{J}| - 1)! |\mathcal{J}|!}{L!} [\widehat{c}(\mathcal{J} \cup \{\ell\}) - \widehat{c}(\mathcal{J})] \\
&= \sum_{\mathcal{J} \subset \mathcal{L}/\{\ell\}} \frac{(L - |\mathcal{J}| - 1)! |\mathcal{J}|!}{L!} \left[\underbrace{\lim_{m \rightarrow \infty} \lim_{B \rightarrow \infty} m\widehat{c}(\mathcal{J} \cup \{\ell\})}_{\textcircled{1}} - \underbrace{\lim_{m \rightarrow \infty} \lim_{B \rightarrow \infty} m\widehat{c}(\mathcal{J})}_{\textcircled{2}} \right]
\end{aligned}$$

Therefore, to show the scaled consistency of \widehat{s}_ℓ for $\ell = 1, 2, \dots, L$, we need to study the scaled consistency of cost function $\textcircled{1}$: $\widehat{c}(\mathcal{J} \cup \{\ell\})$ and $\textcircled{2}$: $\widehat{c}(\mathcal{J})$.

For $\widehat{c}(\mathcal{J})$, based on the multivariate central limit theorem, we have as $m \rightarrow \infty$,

$$\sqrt{m}(\mathbf{X}_{\mathcal{J}}^* - \mathbf{x}_c) \xrightarrow{D} \mathbf{N}(\mathbf{0}_{d \times 1}, \Lambda^*)$$

where $\mathbf{X}_{\mathcal{J}}^* = [\mathbf{X}_{\mathcal{J}}^\top, \mathbf{x}_{c,-\mathcal{J}}^\top]^\top$, $\Lambda^* = \begin{bmatrix} \Lambda_{\mathcal{J}} & 0 \\ 0 & 0 \end{bmatrix}$ and $\Lambda_{\mathcal{J}}$ denotes sub-matrix of Λ with respect to subset $\mathbf{X}_{\mathcal{J}}$.

Since the condition of Theorem 13.1 in [28] still holds, we have

$$\sqrt{m}(m_p(\mathbf{X}_{\mathcal{J}}^*) - m_p(\mathbf{x}_c)) \xrightarrow{D} \mathbf{N}(0, \sigma_{\mathcal{J}}^2)$$

where $\sigma_{\mathcal{J}}^2 = \nabla_{\mathcal{J}} m_p(\mathbf{x}_c)^\top \Lambda_{\mathcal{J}} \nabla_{\mathcal{J}} m_p(\mathbf{x}_c) > 0$, $\nabla_{\mathcal{J}}$ is gradient with respect to subset $\mathbf{X}_{\mathcal{J}}$. This establishes the constant. Moreover, the Condition (14) of Theorem 3.8 of [29] holds. Thus, the cost function estimator $\widehat{c}(\mathcal{J})$ is strongly consistent: $\lim_{m \rightarrow \infty} \lim_{B \rightarrow \infty} m\widehat{c}(\mathcal{J}) = \sigma_{\mathcal{J}}^2$ almost surely.

Similarly, we can prove the cost function estimator $\widehat{c}(\mathcal{J} \cup \{\ell\})$ is also strongly consistent: $\lim_{m \rightarrow \infty} \lim_{B \rightarrow \infty} m\widehat{c}(\mathcal{J} \cup \{\ell\}) = \sigma_{\mathcal{J} \cup \{\ell\}}^2$ almost surely, where $\sigma_{\mathcal{J} \cup \{\ell\}}^2 = \nabla_{\mathcal{J} \cup \{\ell\}} m_p(\mathbf{x}_c)^\top \Lambda_{\mathcal{J} \cup \{\ell\}} \nabla_{\mathcal{J} \cup \{\ell\}} m_p(\mathbf{x}_c) > 0$, $\nabla_{\mathcal{J} \cup \{\ell\}}$ is gradient with respect to $\mathbf{X}_{\mathcal{J} \cup \{\ell\}}$, and $\Lambda_{\mathcal{J} \cup \{\ell\}}$ is sub-matrix of Λ with respect to $\mathbf{X}_{\mathcal{J} \cup \{\ell\}}$.

Consequently, we have Sharpley Value estimator \widehat{s}_ℓ is strongly consistent:

$$\lim_{m \rightarrow \infty} \lim_{B \rightarrow \infty} m\widehat{s}_\ell = \sigma_s^2, \quad \text{with } \sigma_s^2 = \sum_{\mathcal{J} \subset \mathcal{L}/\{\ell\}} \frac{(L - |\mathcal{J}| - 1)! |\mathcal{J}|!}{L!} [\sigma_{\mathcal{J} \cup \{\ell\}}^2 - \sigma_{\mathcal{J}}^2]$$

almost surely.

Next, we will show:

$$\lim_{m \rightarrow \infty} ms_\ell = \sigma_s^2$$

First, we need to show $\lim_{m \rightarrow \infty} mc(\mathcal{J}) = \sigma_{\mathcal{J}}^2$. Let $L(\mathbf{X}_{\mathcal{J}}^*, \mathbf{x}_c)$ denote the line segment joining $\mathbf{X}_{\mathcal{J}}^*$ and \mathbf{x}_c . According to the Multivariate Taylor Formula [27],

$$\begin{aligned}
m_p(\mathbf{X}_{\mathcal{J}}^*) &= m_p(\mathbf{x}_c) + \nabla m_p(\mathbf{x}_c)^\top (\mathbf{X}_{\mathcal{J}}^* - \mathbf{x}_c) \\
&\quad + \frac{1}{2} (\mathbf{X}_{\mathcal{J}}^* - \mathbf{x}_c)^\top \nabla^2 m_p(\mathbf{x}_c) (\mathbf{X}_{\mathcal{J}}^* - \mathbf{x}_c) + \mathcal{R}(\mathbf{X}_{\mathcal{J}}^*, \mathbf{x}_c).
\end{aligned}$$

And the remainder term

$$\mathcal{R}(\mathbf{X}_{\mathcal{J}}^*, \mathbf{x}_c) = \frac{1}{3!} \sum_{i_1=1}^{d_{\mathcal{J}}} \sum_{i_2=1}^{d_{\mathcal{J}}} \sum_{i_3=1}^{d_{\mathcal{J}}} \left. \frac{\partial^3 m_p(x_1, \dots, x_d)}{\partial x_{i_1} \partial x_{i_2} \partial x_{i_3}} \right|_{\mathbf{x}=\mathbf{z}} \prod_{j=1}^3 (X_{\mathcal{J},i_j}^* - x_{c,i_j})$$

where $d_{\mathcal{J}} = \sum_{\ell \in \mathcal{J}} h_{\ell}$, \mathbf{z} denotes a value in the interior of $L(\mathbf{X}_{\mathcal{J}}^*, \mathbf{x}_c)$, and $X_{\mathcal{J},i}$ and $x_{c,i}$ denote the i th components of the vectors $\mathbf{X}_{\mathcal{J}}^*$ and \mathbf{x}_c .

Following the same procedure of **Theorem 4.2.**'s proof, we can obtain

$$[\mathbb{E}[m_p(\mathbf{X}_{\mathcal{J}}^*)]]^2 = m_p^2(\mathbf{x}_c) + m_p(\mathbf{x}_c) \mathbb{E}[(\mathbf{X}_{\mathcal{J}}^* - \mathbf{x}_c)^{\top} \nabla^2 m_p(\mathbf{x}_c) (\mathbf{X}_{\mathcal{J}}^* - \mathbf{x}_c)] + O\left(\frac{1}{m^2}\right).$$

and

$$\begin{aligned} \mathbb{E}[m_p^2(\mathbf{X}_{\mathcal{J}}^*)] &= m_p^2(\mathbf{x}_c) + \mathbb{E}\left[(\mathbf{X}_{\mathcal{J}}^* - \mathbf{x}_c)^{\top} \nabla m_p(\mathbf{x}_c) \nabla m_p(\mathbf{x}_c)^{\top} (\mathbf{X}_{\mathcal{J}}^* - \mathbf{x}_c)\right. \\ &\quad \left. + (\mathbf{X}_{\mathcal{J}}^* - \mathbf{x}_c)^{\top} m_p(\mathbf{x}_c) \nabla^2 m_p(\mathbf{x}_c) (\mathbf{X}_{\mathcal{J}}^* - \mathbf{x}_c)\right] + O\left(\frac{1}{m^2}\right). \end{aligned}$$

Then,

$$\begin{aligned} \text{Var}[m_p(\mathbf{X}_{\mathcal{J}}^*)] &= \mathbb{E}[m_p^2(\mathbf{X}_{\mathcal{J}}^*)] - \left(\mathbb{E}[m_p(\mathbf{X}_{\mathcal{J}}^*)]\right)^2 \\ &= \frac{1}{m} \nabla m_p(\mathbf{x}_c)^{\top} \Lambda^* \nabla m_p(\mathbf{x}_c) + O\left(\frac{1}{m^2}\right). \\ &= \frac{1}{m} \nabla_{\mathcal{J}} m_p(\mathbf{x}_c)^{\top} \Lambda_{\mathcal{J}} \nabla_{\mathcal{J}} m_p(\mathbf{x}_c) + O\left(\frac{1}{m^2}\right). \end{aligned}$$

Therefore, we have $\lim_{m \rightarrow \infty} mc(\mathcal{J}) = \sigma_{\mathcal{J}}^2$. Similarly, we obtain $\lim_{m \rightarrow \infty} mc(\mathcal{J} \cup \{\ell\}) = \sigma_{\mathcal{J} \cup \{\ell\}}^2$. Finally, by applying continuous mapping theorem, we have $\lim_{m \rightarrow \infty} ms_{\ell} = \sigma_s^2$ \square

Remark: The independent variables in our stochastic kriging metamodel consist of central moments and standardized central moments, rather than raw moments. However, Theorem 3 can easily be extended to central and standardized central moments as follows.

Since standardized moments are continuous functions of raw moments, denoted generically as $g(\cdot)$, we can consider the composite function $(m_p \circ g)(\cdot)$ and follow steps analogous to those in the proof of Theorem 3. Up to the third derivatives we have

$$\begin{aligned} (m_p \circ g)'(t) &= m_p'(g(t))g'(t) \\ (m_p \circ g)''(t) &= m_p''(g(t))[g'(t)]^2 + m_p'(g(t))g''(t) \\ (m_p \circ g)^{(3)}(t) &= m_p^{(3)}(g(t))[g'(t)]^3 + 2m_p''(g(t))g'(t)g''(t) \\ &\quad + m_p'''(g(t))g'(t)g''(t) + m_p'(g(t))g^{(3)}(t). \end{aligned}$$

Let u denote the mean, u'_i denote the i th order raw moment and u_i denote the i th order central moment. Then the first three central moments can be expressed as functions of raw moments as follows:

$$\begin{aligned} u_1 &= u, \\ u_2 &= u'_2 - u^2 \\ u_3 &= u'_3 - 3uu'_2 + 2u^3. \end{aligned}$$

The first three standardized central moments are u_1 , $\sqrt{u_2}$ and $u_3/u_2^{3/2}$. For a non-degenerate distribution, the second central moment is positive and bounded away from 0. Thus, the first three derivatives g' , g'' , $g^{(3)}$ exist and are finite.

D Experiment Design

To fit SK metamodels we recommend the experiment design developed in [3] which demonstrated robust performance over a number of test examples. In this section, we briefly review the basic methodology; for detailed information please refer to [3].

The experiment design is not specified a priori; instead the design space, denoted by \mathcal{D} , depends on the real-world data $\mathbf{z}_m^{(0)}$ that will eventually be resampled. In this way the design is adaptive.

At a high level, this is the approach: Generate a large number of bootstrap samples from the real-world data $\mathbf{z}_m^{(0)}$ and compute the corresponding sample moments. Find a regular region that encompasses a large fraction of this sample; this will be the design space. Generate additional bootstrap samples to test that the regular region does indeed cover the desired fraction of the feasible space of sample moments, and refine if necessary. Once satisfied, embed a space-filling design in the regular region. These design points correspond to input distribution moments at which to run simulation experiments to fit the SK metamodel. We provide some more details below.

Suppose we are interested in a $(1-\alpha)100\%$ CI; we set $\alpha = 0.05$ in our empirical study. We want the experiment design to lead to a metamodel that is accurate for moments \mathbf{x} that are the most likely bootstrap moment vectors generated from $\mathbf{z}_m^{(0)}$; by “likely” we mean, for instance, covering $q = 99\% > (1 - \alpha)100\% = 95\%$ of the feasible bootstrap moments.

To this end we find an ellipsoid that will contain an independent bootstrap moment vector obtained by random sampling from $\mathbf{z}_m^{(0)}$ with probability at least q . We then generate a space-filling experiment design inside this ellipsoid. The procedure for constructing the design is as follows:

1. Generate B_0 bootstrap resamples from $\mathbf{z}_m^{(0)}$ and compute the corresponding sample moments to generate a set of sample moments $D_T = \{\widehat{\mathbf{X}}_m^{(b)}, b = 1, 2, \dots, B_0\}$.
2. Find the smallest ellipsoid E such that it contains the fraction q of the data in D_T when the ellipsoid’s center and shape are the sample mean and covariance matrix, respectively, of the elements of D_T .
3. Perform a hypothesis test where the null hypothesis is that a bootstrap moment will be contained in this ellipsoid with probability at least q . This requires computing the number of bootstrap moment resamples, denoted by B_1 , and the constant c that defines the rejection region to attain the desired Type I error and power for the test.
4. Generate B_1 additional independent bootstrap resamples from $\mathbf{z}_m^{(0)}$ and compute the moments $\widehat{\mathbf{X}}_m^{(b)}, b = B_0 + 1, B_0 + 2, \dots, B_0 + B_1$. If more than c of these B_1 resamples are contained in the ellipsoid, then accept the current E as the design space. Otherwise, add these bootstrap resamples to D_T , let $B_0 \leftarrow B_0 + B_1$ and go to Step 2 to update the ellipsoid.
5. Generate k space-filling design points in the ellipsoid E . To place design points into this space, we employ an algorithm due to [32], §3.2.1, for generating points uniformly distributed in an ellipsoid. The algorithm first generates the polar coordinates of a point uniformly distributed in a hypersphere, then transforms it to Cartesian coordinates, and finally transforms it again to a point uniformly distributed in an ellipsoid. The advantage of this approach is that each element of the initial polar coordinates are independently distributed, allowing them to be generated coordinate by coordinate via their inverse cumulative distribution function. Rather than use randomly chosen points, however, we begin with a Latin hypercube sample on $(0, 1)^d$.
6. Assign $n = N/k$ replications to each design point, where N denotes total computational budget. Together the transformed Latin hypercube design points and the number of replications n define the experiment design \mathcal{D} .

In our experiments we set Type I error of the hypothesis test to 0.005 and its power to 0.95 when the true probability is $q = 0.97$.

E Queueing Network Example

In this section we use an queueing network example in Figure 2 to evaluate the performance of our uncertainty analysis framework. Consider estimating the steady state expected number of customers in this network. The interarrival times follow a gamma distribution, $A \sim \text{gamma}(\alpha_A, \beta_A)$, and the service times at the i th station also follow a gamma distribution, $S_i \sim \text{gamma}(\alpha_{S_i}, \beta_{S_i})$. Customers finishing service at stations 1, 2, 3 must make decisions about their next station. These routing decisions follow Bernoulli distributions $P_i \sim \text{Ber}(p_i), i = 1, 2, 3$. The parameters of the input distributions, $\alpha_A, \beta_A, \{(\alpha_{S_i}, \beta_{S_i}), i = 1, 2, 3, 4\}$ and $\{p_i, i = 1, 2, 3\}$ are all unknown and estimated from real-world data. Our goal is to estimate the steady-state expected number of customers in the system when the input parameters assume their true but unknown values.

Both interarrival and service times follow gamma distributions and the routing decisions follow Bernoulli distributions. Thus, it is a 13-dimensional problem with $L = 8$ input processes that include both continuous and discrete

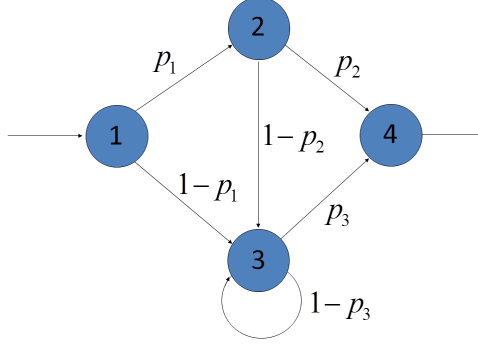


Figure 2: Queueing network example.

distributions. The true model parameters are $\alpha_A = 1, \beta_A = 0.25, \alpha_{S_i} = 1, \beta_{S_i} = 0.2$ for $i = 1, 2, 3, 4$ and $p_1 = p_2 = 0.5, p_3 = 0.75$. These parameter values imply a tractable Jackson network with steady-state number of customers in system $\mu(\mathbf{x}_c) = 12.67$.

In the experiments we assume that all input model parameters are unknown and are estimated from a finite sample of real-world data. Notice that $\alpha_A, \beta_A, \alpha_{S_i}, \beta_{S_i}$ for $i = 1, 2, 3, 4$ are estimated from continuous measurements, while the routing probabilities p_1, p_2, p_3 are estimated from 0 or 1 observations that would correspond to customer routing decisions. The model with *estimated* input parameters is almost surely not a Jackson network and it could be unstable. Our measure of uncertainty is a 95% CI for $\mu(\mathbf{x}_c)$ as defined by (3) because this is the objective desired in practice.

To evaluate the robustness of the metamodel-assisted bootstrapping approach, we systematically examine the effect of the quantity of real-world data and the number of design points and replications per design point used to fit the metamodel; We consider a wide range for the quantity of real-world data $m = 50, 500, 5000$, letting $m_\ell = m$ for $\ell = 1, 2, \dots, L$. The levels for the number of design points are $k = 20, 40, 80, 130$. For a 13-dimensional problem $k = 20$ is a very small design. The studies by [14] and [19] recommend that the number of design points should be 10 times the dimension of the problem for kriging; we take this as the maximum number of design points. The same number of replications are assigned to all design points and we try $n = 10, 50, 100$.

[3] demonstrated that CI_0 has good performance when the impact of metamodel or simulation uncertainty is negligible. In this empirical study we focus on situations where metamodel uncertainty may be significant. However, rather than creating a problem that actually takes hours or days to run, we instead construct a problem with high metamodel uncertainty by using short run lengths for each replication: 20 time units after the warm up, which is roughly equivalent to 80 finished customers. To avoid the influence from initial bias, all simulations start loaded with the number of customers at each station being their steady-state expected values (rounded) under \mathbf{x}_c . Furthermore, a long warmup period of 200 time units is used. The net effect is that the point estimators of the steady-state number in the network have low bias, but may be quite variable.

E.1 Performance of CIs

A fundamental assumption of simulation is that the expectation $\mu(\mathbf{x}_c)$ exists. This assumption does not imply, however, that it exists for *all* possible values of \mathbf{x} , \mathbf{X}_m or $\widehat{\mathbf{X}}_m^{(b)}$ that might be realized. The prototype example is a congestion-related performance measure of a queueing system as time goes to infinity when congestion increases without bound for some values of its interarrival-time and service-time parameters. We refer to systems for which $\mu(\mathbf{x})$ is $\pm\infty$ for some values of \mathbf{x} as potentially *unstable*. The conditional probability that a bootstrap resampled moment $\widehat{\mathbf{X}}_m^{(b)}$ is located in the unstable region, denoted by U , given the real-world data is

$$P_U \equiv \Pr \left\{ \widehat{\mathbf{X}}_m^{(b)} \in U \mid \mathbf{z}_m^{(0)} \right\}. \quad (34)$$

Since P_U only depends on m and \mathbf{x}_c , we ran a side experiment to estimate it using

$$\widehat{P}_U = \frac{1}{B} \sum_{b=1}^B \mathbf{I} \left(\widehat{\mathbf{X}}_m^{(b)} \in U \right), \quad (35)$$

where $\mathbf{I}(\cdot)$ is the indicator function. The means and standard deviations (SD) of \widehat{P}_U for $m = 50, 500, 5000$ were estimated based on 1000 macro-replications and are displayed in Table 6. In each macro-replication we independently

Table 6: Percentage of unstable bootstrap resampled moments.

	$m = 50$	$m = 500$	$m = 5000$
mean of \widehat{P}_U	44.4%	2.3%	0
SD of \widehat{P}_U	31.7%	7.9%	0

Table 7: Results for CI_0 , CI_+ and $\widehat{\sigma}_I/\widehat{\sigma}_T$ when $m = 50$.

$m = 50$	$k = 20$			$k = 40$		
	$n = 10$	$n = 50$	$n = 100$	$n = 10$	$n = 50$	$n = 100$
Coverage of CI_0	91.9%	92.3%	91.5%	93.8%	94.4%	93.4%
Coverage of CI_+	93.9%	94.9%	93.7%	94.9%	95.6%	95.9%
CI_0 Width (mean)	326.4	332.4	339.5	319.1	328.6	326.5
CI_+ Width (mean)	344.1	348.8	357.1	332.3	342.3	341.2
CI_0 Width (SD)	183.1	173.6	180.7	176.4	167.6	175
CI_+ Width (SD)	188	175.7	183.8	178.2	169.2	176.1
$\widehat{\sigma}_I/\widehat{\sigma}_T$	0.963	0.965	0.964	0.973	0.973	0.971

$m = 50$	$k = 80$			$k = 130$		
	$n = 10$	$n = 50$	$n = 100$	$n = 10$	$n = 50$	$n = 100$
Coverage of CI_0	94.6%	96.3%	95.4%	94.2%	95.1%	95.4%
Coverage of CI_+	95.9%	96.7%	96.1%	94.5%	96%	96.1%
CI_0 Width (mean)	312.1	314.8	322.7	322	321.86	320
CI_+ Width (mean)	322	325.7	334	330.2	331	329.4
CI_0 Width (SD)	169.7	159.1	164.7	171.5	169.3	172.3
CI_+ Width (SD)	171.2	159.4	165	172.7	169.5	172.7
$\widehat{\sigma}_I/\widehat{\sigma}_T$	0.982	0.98	0.978	0.985	0.985	0.983

generated a sample of size m of “real-world data.” Then, conditional on these data, we drew $B = 2000$ bootstrap resampled moments.

As m increases the bootstrap resampled moments become more closely centered around \mathbf{x}_c . Thus, both the mean and SD of \widehat{P}_U decrease with increasing m as shown in Table 6. When $m = 50$, P_U appears to be much larger than $\alpha/2$ so the bootstrap moments $\widehat{\mathbf{X}}_m^{(b)}$ that correspond to the upper confidence bound are located in the unstable region U with high probability. When $m = 500$, P_U appears to be close to $\alpha/2 = 2.5\%$, while when $m = 5000$ there is little chance of getting unstable bootstrap moments.

Tables 7–8 show the results for CI_0 and CI_+ when $m = 50, 500, 5000$, including the probability of covering $\mu(\mathbf{x}_c)$, and the mean and SD of the interval widths. All results are based on 1000 macro-replications. When $m = 50$, P_U is much greater than $\alpha/2$ according to Table 6. This explains the very large CI widths in Table 7. Nevertheless, both CI_0 and CI_+ have reasonable coverage overall. Notice that CI_0 does exhibit undercoverage when we use a very small experiment design of $k = 20$ points, while the coverage of CI_+ is much closer to the nominal value of 95% in this case. If we fix the number of replications n and increase the number of design points k , the coverage of CI_0 improves. For a fixed k the effect of increasing n is not as obvious.

Table 8 shows the results for $m = 500, 5000$. Compared with the results for $m = 50$, the mean and SD of the interval widths drop dramatically. The effects of k and n are easier to discern especially when $m = 5000$, which has no unstable bootstrap moments. Specifically, for a fixed quantity of real-world data m , if either the number of design points k or replications per design point n is small then CI_0 tends to have undercoverage because it fails to account for substantial simulation uncertainty. The most troubling observation about CI_0 is that, for fixed (n, k) , as the amount of input data m increases its undercoverage becomes more serious. The diminished coverage occurs because as $m \rightarrow \infty$ the width of CI_0 shrinks to zero, which is not appropriate when there is still simulation uncertainty. As the interval, CI_+ , is able to account for the effect of the remaining simulation estimation error, it can work under more general situations where the simulated systems are complex and the simulation budget is tight. As n and k increase, the coverages of CI_0 and CI_+ become closer to each other.

E.2 Performance of $\widehat{\sigma}_I/\widehat{\sigma}_T$

Tables 7–8 also demonstrate that $\widehat{\sigma}_I/\widehat{\sigma}_T$ provides a good measure of the relative contribution of model uncertainty to overall uncertainty. For a fixed amount of real-world data m , increasing the number of design points and replications

Table 8: Results of the queueing network example for CI_0 , CI_+ and $\hat{\sigma}_I/\hat{\sigma}_T$ when $m = 500$ and $m = 5000$.

$m = 500$	$k = 20$			$k = 40$		
	$n = 10$	$n = 50$	$n = 100$	$n = 10$	$n = 50$	$n = 100$
Coverage of CI_0	90.5%	94.6%	95.1%	94.9%	96.7%	96.4%
Coverage of CI_+	95.7%	97.7%	97.8%	96.6%	98.3%	97.8%
CI_0 Width (mean)	24.8	28.1	29.4	27.1	28.5	28.7
CI_+ Width (mean)	28.9	30.8	32.2	29.6	30.3	30.5
CI_0 Width (SD)	19.9	19.4	20.6	19.1	19.2	19.9
CI_+ Width (SD)	20.6	20.4	21.7	19.7	19.9	20.6
$\hat{\sigma}_I/\hat{\sigma}_T$	0.88	0.932	0.933	0.932	0.957	0.958
$m = 500$	$k = 80$			$k = 130$		
	$n = 10$	$n = 50$	$n = 100$	$n = 10$	$n = 50$	$n = 100$
Coverage of CI_0	96.5%	97.5%	95.8%	95.4%	96.5%	95.9%
Coverage of CI_+	98%	98.3%	97.3%	97.5%	97.1%	96.9%
CI_0 Width (mean)	26.3	28	28.7	26.4	27.9	27.6
CI_+ Width (mean)	28	29	29.7	27.9	28.6	28.2
CI_0 Width (SD)	17.4	18	19.3	18.8	19.6	19.3
CI_+ Width (SD)	17.7	18.4	19.6	18.9	19.9	19.5
$\hat{\sigma}_I/\hat{\sigma}_T$	0.952	0.977	0.978	0.957	0.984	0.987
$m = 5000$	$k = 20$			$k = 40$		
	$n = 10$	$n = 50$	$n = 100$	$n = 10$	$n = 50$	$n = 100$
Coverage of CI_0	70.7%	89.2%	93.1%	81.5%	94.3%	94.8%
Coverage of CI_+	91.3%	96.3%	95.6%	96.5%	96.1%	96.3%
CI_0 Width (mean)	3.29	3.97	4.14	3.93	4.23	4.3
CI_+ Width (mean)	5.85	4.8	4.56	6.08	4.64	4.52
CI_0 Width (SD)	1.89	1.2	1	1.64	0.87	0.83
CI_+ Width (SD)	2.12	1.13	1	1.52	0.89	0.85
$\hat{\sigma}_I/\hat{\sigma}_T$	0.588	0.85	0.924	0.664	0.924	0.959
$m = 5000$	$k = 80$			$k = 130$		
	$n = 10$	$n = 50$	$n = 100$	$n = 10$	$n = 50$	$n = 100$
Coverage of CI_0	88.9%	93.6%	94.9%	89.5%	93.7%	94.8%
Coverage of CI_+	98.1%	95%	96%	98%	95.6%	95.5%
CI_0 Width (mean)	4.54	4.29	4.29	4.52	4.35	4.32
CI_+ Width (mean)	6.1	4.56	4.42	5.98	4.64	4.45
CI_0 Width (SD)	1.37	0.85	0.77	1.28	0.9	0.79
CI_+ Width (SD)	1.27	0.85	0.78	1.13	0.87	0.77
$\hat{\sigma}_I/\hat{\sigma}_T$	0.757	0.946	0.974	0.766	0.945	0.974

(n, k) drives $\hat{\sigma}_I/\hat{\sigma}_T$ toward 1, indicating a decrease in simulation uncertainty. For fixed simulation effort (n, k) , increasing the amount of real-world data m decreases $\hat{\sigma}_I/\hat{\sigma}_T$, indicating that there is relatively less model uncertainty. Notice, however, that the relationship is not simple because as m increases the design space over which we fit the metamodel becomes smaller, so that even with the same simulation effort the absolute level of simulation uncertainty will decrease somewhat. When $\hat{\sigma}_I/\hat{\sigma}_T$ is near 1, the behaviors (coverage and width) of CI_0 and CI_+ are similar and both have coverage close to the nominal level; this is illustrated in Figure 3. Recall that CI_0 does not account for simulation uncertainty, and that $\hat{\sigma}_I/\hat{\sigma}_T \approx 1$ indicates that model uncertainty is large relative to simulation uncertainty, which is when CI_0 will do best. Figure 3 also illustrates the general robustness of CI_+ .

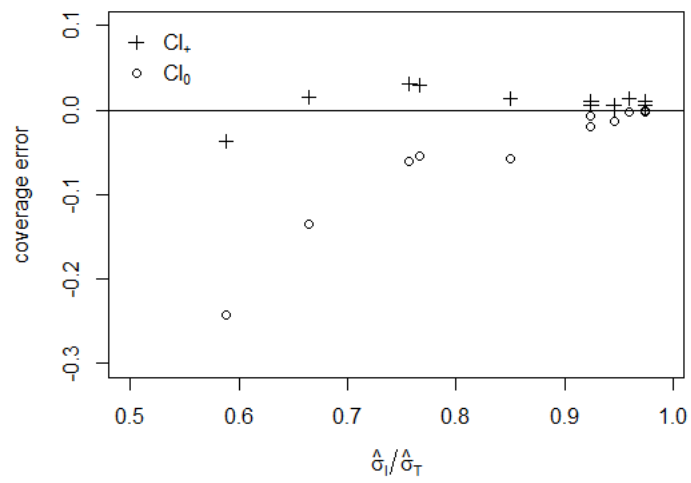


Figure 3: The coverage errors for CI_0 and CI_+ vs. $\hat{\sigma}_I / \hat{\sigma}_T$ when $m = 5000$ across all values of n and k .